Atmospheric
Chemistry
and Physics
Discussions

The role of nanoparticles in Arctic cloud formation

Linn Karlsson[1,2], Radovan Krejci[1,2], Makoto Koike[3], Kerstin Ebell[4], and Paul Zieger[1,2]

[1]Department of Environmental Science, Stockholm University, Stockholm, Sweden
[2]Bolin Centre for Climate Research, Stockholm University, Stockholm, Sweden
[3]Department of Earth and Planetary Science, University of Tokyo, Tokyo, Japan
[4]Institute for Geophysics and Meteorology, University of Cologne, Cologne, Germany

Correspondence: Paul Zieger (paul.zieger@aces.su.se)

Abstract. To constrain uncertainties in radiative forcings associated with aerosol–cloud interactions, improved understanding of Arctic cloud formation is required, yet long-term measurements of the relevant cloud and aerosol properties remain sparse. We present the first long-term study of cloud residuals, i.e. particles that were involved in cloud formation, and ambient aerosol particles in Arctic low-level clouds measured at Zeppelin Observatory, Svalbard. A detailed evaluation of the ground-based

5 counter-flow virtual impactor inlet system is also presented. Cloud residuals as small as 15 nm are routinely observed especially during the dark period and are potentially linked to ice, supporting prior work suggesting that classical droplet activation is not the only relevant process in the formation of Arctic low-level clouds. The reported measurements and findings provide a new basis for improving our understanding of Arctic clouds and for developing robust parameterisations of mixed-phase clouds in Earth system models.

10 **1 Introduction**

Aerosols and clouds are important for climate, yet they remain one of the largest sources of uncertainty in climate projections (Boucher et al., 2013). Many of the parameters that govern cloud and aerosol formation are subject to change as the climate changes as well, which further obscures the picture. The Arctic is a region of particular interest, because it is warming more rapidly than the rest of the globe (Serreze and Francis, 2006; Serreze and Barry, 2011). In terms of aerosol particles, the

15 Arctic is characterised by a distinct seasonal cycle with low natural background number concentrations for parts of the year Willis et al. (2018). The low background concentration is especially true for late autumn and early winter when the absence of sunlight and direct particle sources inhibits natural emissions and the formation of new particles (Tunved et al., 2013). This means that small changes in Arctic aerosol particle concentrations, for example following sea ice loss and increased natural marine emissions (Struthers et al., 2011) or altered transport and/or emissions of anthropogenic particles (Law and Stohl, 2007),

20 can potentially cause large changes in cloud properties (Mauritsen et al., 2011). Crucially, the autumn and winter seasons are also when Arctic amplification is most pronounced (Serreze and Barry, 2011; Maturilli and Kayser, 2017), which makes such changes more likely to happen. Due to the sparsity of observations, we know less about cloud and aerosol processes in the Arctic than elsewhere. New long-term observations are thus essential for closing existing knowledge gaps.

Long-term observations of Arctic aerosol particles generally come from a relatively small number of permanent measurement stations. While there are differences in aerosol properties between the sites, it has been shown that they all share common features both in terms of particle number concentration and particle number size distribution (Freud et al., 2017). This characteristic seasonal cycle of Arctic aerosol properties has been demonstrated previously for individual sites (Ström et al., 2003; Tunved et al., 2013; Nguyen et al., 2016). During the transition from winter to springtime, the number concentration of accumulation mode particles (typically diameter > 60 nm) increases due to long-range transport of polluted air masses – a phenomenon known as Arctic haze (Mitchell, 1956). In summer, changes in circulation and cloud cover lead to efficient scavenging of these particles, subsequently lowering their concentration (Tunved et al., 2013). Lower accumulation mode particle concentrations, together with increased biological activity and photochemistry, helps facilitate new particle formation leading to number size distributions dominated by the smaller, Aitken mode particles (typically diameter < 60 nm) in the Arctic summertime (Ström et al., 2003). During autumn, the particle sinks are stronger than the sources because neither transport nor new particle formation is efficient, which leads to low number concentrations across the particle size spectrum (Tunved et al., 2013).

Studies characterising Arctic cloud condensation nuclei (CCN) generally cover short time periods, and only a couple of studies exist that look at the seasonal cycle in the Arctic (Jung et al., 2018; Dall'Osto et al., 2017; Schmale et al., 2018). Jung et al. (2018) measured CCN on Svalbard and found that the seasonal variation in CCN concentrations correlated well with the variation in accumulation mode aerosol particle concentrations. They also identified new particle formation and subsequent particle growth as contributors to summertime CCN concentrations, in line with results from a previous long-term study (Dall'Osto et al., 2017) as well as shorter airborne and ground-based measurement campaigns (Leaitch et al., 2016; Zábori et al., 2015). CCN number concentrations in the Arctic have been found to range between a few tens and a couple of hundred particles cm^{-3} (Jung et al., 2018), although concentrations vary spatially. Local concentrations of less than 1 and more than 1000 cm^{-3} have been reported (Mauritsen et al., 2011; Moore et al., 2011). CCN are of course only part of the picture – in cold and mixed-phase clouds, ice nucleating particles (INP) are also important. INP are much rarer, with concentrations several orders of magnitude lower than typical CCN concentrations. In the Arctic, INP concentrations have been found to range between approximately 10^{-5} and 10^{-1} L^{-1} (see e.g., Wex et al., 2019; Tobo et al., 2019; Irish et al., 2019).

An important caveat is that all of the aforementioned studies measure CCN and INP concentrations by artificially activating aerosol particles. It is, however, possible to study CCN and INP properties directly inside clouds, by measuring the so-called cloud residuals that remain when cloud droplets and ice crystals (collectively termed cloud particles) are dried. This can for example be achieved with a counterflow virtual impactor (CVI) inlet (Ogren et al., 1985; Noone et al., 1988), which separates cloud particles from unactivated aerosol particles on an inertial basis. Because the CVI can measure both water and ice particles, cloud residuals may correspond to either CCN or INP. In the Arctic, CVI inlets have previously only been deployed during short, dedicated aircraft campaigns (McFarquhar et al., 2011; Wendisch et al., 2019) and, until now, no long-term observations of cloud residual properties have been performed either in the Arctic or globally. Here, we present a unique dataset of size-resolved cloud residual number concentrations recorded between 2015 and 2018 at Zeppelin Observatory on Svalbard using a ground-based CVI inlet. These are the first continuous measurements of cloud residuals in the Arctic that cover the full annual cycle. Our observations are accompanied by measurements of total aerosol particles (interstitial and activated aerosol particles)
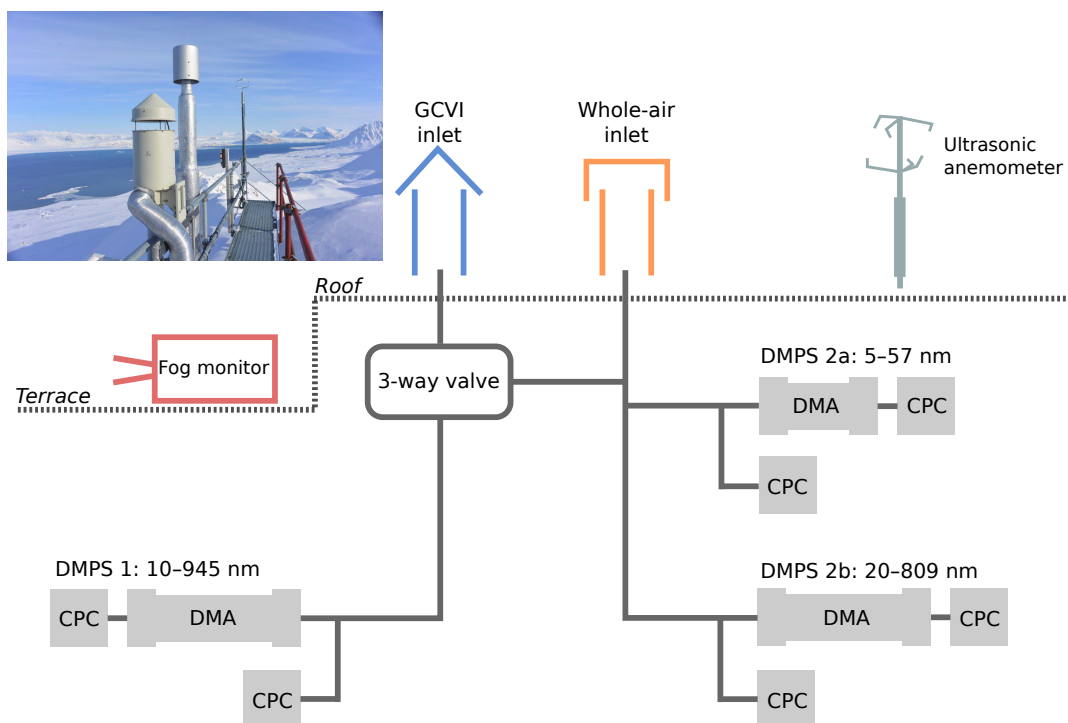
Figure 1. Schematic illustration of the experimental set-up at Zeppelin Observatory. The diagram shows how the whole-air inlet (orange) and the ground-based counterflow virtual impactor (GCVI) inlet (blue) are connected to the differential mobility analysers (DMAs) and condensation particle counters (CPCs). The 3-way valve switches the sample flow to the instruments on the left-hand side from the GCVI inlet to the whole-air inlet when there is no cloud to be sampled. Cloud sampling is activated if the visibility drops below 1 km (measured by a visibility sensor (not pictured) next to the GCVI inlet). Auxiliary measurements from a fog monitor and an ultrasonic anemometer have also been included in the data analysis.

and ambient cloud particle size distributions, meteorological parameters as well as remote sensing data, which, taken together,

60 provide valuable new information about the elusive Arctic CCN.

2 Methods

We present total particle and cloud residual size distributions and integrated number concentrations measured during more than 2 years (26 November 2015 to 4 February 2018) at Zeppelin Observatory using two different inlet systems. These measurements are complemented by measurements of ambient cloud particle size distributions, temperature, wind parameters and remote

65 sensing data which are described below. A schematic illustration of the experimental set-up and a photo of the inlet systems at Zeppelin Observatory are shown in Fig. 1. Tables 1 and S1 (in the supplementary material) give further details on the instrumentation and data coverage.

2.1 Site description

Zeppelin Observatory (78°54'N 11°53'E) is located on Svalbard in the high Arctic, approximately 2 km south of the research

70 village Ny-Ålesund. Situated 480 m above sea level (inlet height) on the ridge of Mt. Zeppelin, the station is largely unaffected by local pollution sources and often in cloud (∼16 % of the time in 2015–2018, where *in cloud* is defined in this work as visibility < 1 km for at least 5 min as measured by the visibility sensor, see below), making it well-suited for the study of Arctic aerosol particles and clouds. Note that the observed cloud occurrence may not exactly equal the annual mean cloud occurrence at the station, as we have a slightly uneven data coverage for the different months (cf. right panel in Fig. 5).

75 Two predominant wind directions are characteristic for the site: south and north-north-west with a median horizontal and vertical wind speed of $3.0 \, \text{ms}^{-1}$ and $0.7 \, \text{ms}^{-1}$ during periods of cloud occurrence (see Fig. S1 in supplementary material). The annual cycle of aerosol size distribution parameters is quite predictable for the site (Tunved et al., 2013), however, the site can not be regarded as being representative for the entire Arctic. Freud et al. (2017) has shown that although certain similarities in aerosol size and concentration exist between the different permanent measurement sites in the Arctic, e.g. caused by similarities in transport patterns, particle formation or removal mechanisms, distinct differences were attributed to the proximity of aerosol

80 sources, local meteorological effects or the influence of open ocean, land areas and sea ice.

In terms of cloud cover and cloud type, it is difficult to say how representative the measurements at Ny-Ålesund and Zeppelin Observatory are for the broader Arctic. Shupe et al. (2011) have analyzed the occurrence and macro-physical properties of Arctic clouds at six observatories, including Ny-Ålesund, and found, for example, that clouds are more persistent at the far

85 western Arctic sites. More detailed analyses of cloud radar observations from Ny-Ålesund (Nomokonova et al., 2019b; Ebell et al., 2020; Nomokonova et al., 2019a; Gierens et al., 2020) partly confirmed results of previous studies, e.g. high a cloud occurrence at Ny-Ålesund in summer and autumn, but also revealed differences. For example, Nomokonova et al. (2019b) revealed a higher annual cloud occurrence at Ny-Ålesund (∼81%) than Shupe et al. (2011, ∼61%). Differences in the observed cloud statistics are likely also due to different observing instruments and methods as well as different time periods analysed.

90 The previously reported cloud occurrences are much higher than what we observe, because we are observing at a fixed altitude and thus only measure low-level clouds. The representativeness of our observational conditions for the broader Arctic cloud cover (cf. Liu et al., 2012) is unclear.

Dahlke and Maturilli (2017) showed that the synoptic flow towards Ny-Ålesund represents typical Arctic climate during the summer months, while during the winter periods large scale advection from lower latitudes is dominating in recent decades,

95 resulting in a more maritime climate. This transition will most likely affect also cloud properties with Ny-Ålesund probably becoming less representative of the Arctic.

2.2 Inlet systems

2.2.1 Whole-air inlet

The standard aerosol inlet is heated and fulfils the World Meteorological Organization (WMO)/Global Atmosphere Watch

100 programme guidelines for aerosol sampling of whole-air (Kazadzis, 2016) and has similar characteristics as the inlet described

by Weingartner et al. (1999) which can sample cloud droplets up to $40\,\mu$m at wind speeds up to $20\,\mathrm{ms^{-1}}$. It is placed on the roof of the station, and particle-laden air is brought into the lab where an isokinetic flow splitter directs the air to the different sampling instruments through quarter inch stainless steel tubing. The air is not actively dried, but the temperature difference between the outside and the inside of the lab causes a reduction in the relative humidity. During our sampling period, the

105 relative humidity of the sample flow was always below $40\,\%$ (mean$\pm$std for our period: $13\pm7\,\%$).

2.2.2 Ground-based counterflow virtual impactor inlet

For sampling of cloud residuals, we utilise a ground-based counterflow virtual impactor (GCVI; Brechtel Manufacturing Inc., USA, Model 1205) inlet, which is based on the working principles described in Noone et al. (1988). The inlet uses opposing air flows to filter out particles with low inertia (i.e. interstitial particles), so that only activated particles (i.e. droplets and ice

110 crystals) are sampled. A detailed technical description of the GCVI can be found in Shingler et al. (2012). Here, we outline the basic principles only.

The GCVI inlet at Zeppelin Observatory is mounted vertically on the north side of the station roof. During operation, cloudy air is accelerated onto the tip of the inlet with the help of a wind tunnel with typical airspeeds of around $120\,\mathrm{ms^{-1}}$ (monitored with a pitot tube). When the ambient air meets the counterflow within the GCVI, two stagnation planes are generated where

115 only particles with sufficient inertia (i.e. cloud droplets or ice crystals) can pass through and enter the sample flow. The sample flow rate is set to $15\,\mathrm{L\,min^{-1}}$ by automatic mass flow controllers that take into account the actual sample flow of each connected instrument. The lower cut-size ($D_{50\%}$) in the inlet is calculated by the instrument software and is determined by the different flow velocities and the distance between the stagnation planes. Shingler et al. (2012) compared experimentally determined cut-sizes to those predicted by the software and found good agreement. The cut-size was generally between 6 and

120 $7\,\mu$m aerodynamic diameter during our sampling period. As the cloud particles travel through the inlet, they are dried until only the cloud residuals remain. Cloud particles larger than approximately $40\,\mu$m in diameter are impacted in a particle trap inside the inlet due to their long evaporation times (Shingler et al., 2012).

The GCVI is only operated when there is a cloud at the station. The system is automated and uses a visibility sensor to determine whether or not a cloud is present. The GCVI is turned on when the visibility drops below 1 km (the WMO's

125 definition of fog). Visibility is the only criterion used, so there is no discrimination between precipitating and non-precipitating clouds. When the visibility is above 1 km, instruments that normally sample behind the GCVI inlet instead receive their sample flow from the whole-air inlet. This is achieved with a three-way valve (installed in April 2017) between the two inlets and the instruments, and allows us to collect duplicate measurements of particle size and concentrations for quality assurance during non-cloud periods.

130 Particles that enter the wind tunnel are concentrated at the tip of the CVI inlet, meaning the sampled air is effectively enriched in cloud particles relative to the ambient air. The concentrations observed behind the GCVI therefore have to be corrected by an enrichment factor (EF), which depends on the airspeed in the wind tunnel, the sample flow rate and the geometry of the inlet itself (Shingler et al., 2012). With our set-up, the EF was 11.9 ± 1 (median 12). It should be emphasised that even after correcting for the EF, the cloud residual concentrations measured behind the GCVI cannot be considered as absolute due to

135   the transmission efficiency of the inlet. Because the transmission efficiency depends on the size of the cloud particles before
they are dried, it cannot be corrected for. However, an estimate of the absolute cloud residual concentrations can be obtained
by back-calculating from the ambient cloud particle size distribution (as measured by a fog monitor) using the experimentally
determined cloud particle size dependent transmission efficiency (Shingler et al., 2012) of the GCVI inlet. As will be shown
below, we find that on average half of the ambient cloud particles make it into the GCVI sample flow, and cloud residual
140   concentrations therefore have to be multiplied by a factor of 2 (see Sect. 3).

2.3   Instrumentation

See Fig. 1 for a schematic overview of the experimental set-up and Table 1 for a summary of the instruments used, parameters
measured and their temporal and/or spatial resolutions.

Table 1. List of instruments, measured parameters and their temporal and/or spatial resoultion.

Instrument	Parameters	Resolution
DMPS 1	Aerosol particle number size distributions (diameters 10–945 nm)	5–7 min
DMPS 2a–b	Aerosol particle number size distributions (diameters 5–809 nm)	15–16 min
GCVI	Visibility (proxy for cloud presence)	1 s
FM-120	Cloud particle number size distributions (diameters 3–47 μm)	10 s
Ultrasonic anemometer (METEK uSonic-3)	3D wind field, virtual temperature	1 s
Cloudnet	Target classification (in terms of occurrence of e.g. liquid droplets, ice crystals, drizzle, etc)	30 s, 20 m altitude bins

2.3.1   Differential mobility particle sizer

145   Particle number size distributions were measured with a differential mobility particle sizer (DMPS). The experimental set-up
at Zeppelin Observatory has three DMPS instruments: one is behind the GCVI inlet (DMPS 1) and the other two are behind the
whole-air inlet (DMPS 2a–b). DMPS 1 (sample flow 1 L min^{-1}, sheath-air flow 4.8 L min^{-1}) consists of a medium Vienna type
differential mobility analyser (DMA; length 0.28 m, outer radius 0.033 m, inner radius 0.025 m) and a condensation particle
counter (CPC; TSI Inc., USA, Model 3772). Another CPC (TSI Inc., USA, Model 3772) is used in parallel with the DMPS
150   to measure the total particle number concentration. DMPS 1 is set to measure particles from 10 to approximately 945 nm in
mobility diameter. A full DMPS 1 scan (small to large or large to small diameters) takes approximately 6 min to complete.

DMPS 2a and DMPS 2b measure different but overlapping size ranges. They are synchronised as one system (DMPS 2a–b)
that runs on the same software. DMPS 2a (sample flow 1 L min^{-1}, sheath-air flow 9.9 L min^{-1}) measures at the smaller end
of the particle size spectrum and has an extra small Vienna type DMA (length 0.053 m, outer radius 0.033 m, inner radius
155   0.025 m) to minimise diffusional losses, with a CPC (TSI Inc., USA, Model 3010) behind the DMA and a CPC (TSI Inc.,
USA, Model 3776) for measuring the total aerosol particle concentration. DMPS 2b (sample flow 1 L min^{-1}, sheath-air flow

5.2 L min^{-1}) measures the larger size particles and has a medium Vienna type DMA (length 0.28 m, outer radius 0.033 m, inner radius 0.025 m) with a CPC (TSI Inc., USA, Model 3772) behind the DMA and a CPC (TSI Inc., USA, Model 3010) for measuring the total aerosol particle concentration. Together, DMPS 2a–b span roughly the same size range as the DMPS 1, but
160   the time resolution is approximately 15 min per full scan.

We have not applied any standard temperature and pressure normalisation or particle shape correction to the data presented here, but multiple-charge corrections have been applied to all measured size distributions. They have also been corrected for particle losses due to diffusion and impaction using the *Particle Loss Calculator* by von der Weiden et al. (2009), assuming a particle density of 1 g cm^{-3}.

165   After a manual data screening to remove outliers and contamination, 1 729 hours of cloud residual number size distribution measurements remained. The full cloud residual data are shown in Figs. 6 and 7; however, for the remaining figures we were limited by the availability of concurrent data from the other instruments (DMPS 2a, DMPS 2b, the fog monitor, the ultrasonic anemometer, and the Cloudnet retrieval). Thus, slightly different subsets of the cloud residual data are used in the different figures. Table S1 shows how many hours of simultaneous measurements we have for different instrument combinations, and
170   which figures the combinations are relevant for.

Figure S2 shows how the DMPS systems compare during non-cloud periods. The comparison is based on data collected from May 2017–February 2018 (after the installation of the three-way inlet valve, see above). In general, the instruments compare well for large particle sizes while DMPS 2a–b shows consistently higher concentrations of small particles below around 30 nm in diameter. This is to be expected, since the diffusion losses are higher for DMPS 1 due to the instrument dimensions and
175   longer sampling lines. These diffusion losses cannot be corrected for when the concentrations in the smaller size bins are zero. Most of the differences originate from the lowest size bins between 10 and 15 nm, as can be seen in the scatter plots of Fig. S2 (panel c and d), where the integrated number concentrations of both DMPS 1 and DMPS 2a–b are shown. The slope of the orthogonal linear regression and the R^2-value improve from 1.36 to 1.01 and 0.96 to 0.99, respectively, if particle number size distributions are integrated above 15 nm instead of 10 nm particle diameter.

180   **2.3.2   Fog monitor**

A fog monitor (Droplet Measurement Technologies Inc., USA, Model FM-120) was used to determine the ambient cloud particle size and number concentration. It uses an optical method to size individual cloud particles at a flow rate of approximately 1000 L min^{-1} (airspeed 12 m s^{-1}). The instrument is positioned facing south and measures ambient cloud particle size distributions in the size range 3.5–46 μm optical diameter (bin midpoints). More details on the instrument at Zeppelin Observatory
185   can be found in Koike et al. (2019). It should be noted that no loss correction has been applied to the fog monitor data because no clear signatures of particle loss were found in previous work by Koike et al. (2019), although significant sampling losses were suggested in other studies depending on, for example, the cloud particle diameter, and the wind speed and wind direction relative to the fog monitor (Spiegel et al., 2012).

2.3.3 Ultrasonic anemometer

190   A uSonic-3 Omni (METEK GmbH) ultrasonic anemometer was used to monitor wind conditions at Zeppelin Observatory. The anemometer has 3 pairs of ultrasonic transducers arranged to form 3 paths along which the speed of sound is measured. From the difference in the travel time of sound along the 3 measuring paths, the 3D wind vector as well as the acoustic temperature can be derived. The acoustic temperature is a close approximation of the virtual temperature, which depends on the ambient relative humidity and is generally 1–2 degrees higher than the true temperature (METEK GmbH, 2013). However, note that

195   at Zeppelin Observatory during our measurement period, the median difference between the measured acoustic temperature and the ambient temperature measured by a Vaisala temperature probe (located in the meteorology mast at 15 m above the measurement platform) was around $3.4°C$. Nevertheless, we chose to use the temperature from our anemometer because we needed the higher time resolution that it provides.

2.3.4 Cloud remote sensing

200   The Cloudnet algorithm suite (Illingworth et al., 2007) has been applied to the Ny-Ålesund ground-based remote sensing observations from the French-German research station AWIPEV (Nomokonova et al., 2019b), which is located approximately 2 km north of Zeppelin Observatory. A standard product is the target classification which combines measurements from cloud radar, ceilometer and microwave radiometer with output from a numerical weather prediction model. Each radar height bin is classified in terms of the occurrence of e.g. liquid droplets, ice particles, rain/drizzle, melting ice and a combination of those.

205   More details on the product for Ny-Ålesund can be found in Nomokonova et al. (2019b). For comparison with the cloud residual data collected at Zeppelin Observatory, we selected Cloudnet height bins between 400 and 600 m. We only compared cases when the cloud base height at AWIPEV was between 300 m and 600 m to ensure that the classifications were likely to be applicable also to the cloud at Zeppelin Observatory. It should be noted that this cloud base height criterion reduces the number of data points we can use, such that we only have Cloudnet data for approximately 30% of our in-cloud size distribution data.

2.4 Cluster analysis

A cluster analysis was performed to identify cloud residual size distributions that were dominated by Aitken mode particles. We used k-means clustering, implemented in the *scikit-learn* (v. 0.20.2) Python package (Pedregosa et al., 2011), which is a method to categorise data into a pre-defined number of clusters, k, where members of a cluster are as similar to each other as possible while at the same time being as different to members of other clusters as possible. Each data point is assigned to

215   the cluster with the nearest mean. We categorised cloud residual number size distributions based on their shape, so the size distributions were normalised by the integral before applying the k-means algorithm. We selected 5 clusters ($k = 5$) to separate out the cloud residual size distributions that were dominated by the very smallest particles. Choosing fewer clusters did not fully separate this distribution of interest, while more clusters led to a further splitting of the accumulation mode (see Fig. S3).

3 Assessment of the GCVI sampling efficiency

220   The ambient cloud particle size distributions were used to evaluate the sampling performance of our GCVI system. Assuming that the cloud particle distribution measured by the FM-120 fog monitor is an accurate representation of the cloud particles that enter the GCVI inlet, we applied the experimentally determined size-dependent transmission efficiency from Shingler et al. (2012) (linearly extrapolated to cover the full FM-120 cloud particle size range) to calculate the cloud particle concentration above the GCVI cut-size that would have made it into the sample flow. Here, it is important to note that the transmission

225   efficiency was determined for hollow glass beads without using the inlet counterflow (Shingler et al., 2012). As such, it does not take into account potential evaporation of water from the cloud particles in the different inlet segments. Within this work, we have only used the transmission efficiency determined for the first inlet segment, because we believe that the dry counterflow initiates evaporation which would make the transmission efficiency determined for subsequent sections an underestimation of the true transmission efficiency. This choice may result in an overestimation of the transmission efficiency (particularly of

230   larger cloud droplets) since some losses are effectively ignored, but no correction is preferable to an invalid correction.

The corrected cloud particle concentrations, integrated above the GCVI cut-size, were compared to the integrated cloud residual number concentrations measured behind the GCVI inlet, and the result can be seen in Fig. 2. Given the uncertainties involved, the instruments agree reasonably well in terms of the seasonal cycle and magnitude of cloud particle/cloud residual concentrations (Fig. 2a). A 2D histogram of corrected cloud particle concentrations versus cloud residual concentrations

235   (Fig. 2b) shows that most of the data points lie on or around the 1:1 line. An orthogonal linear regression of cloud residual versus cloud particle number concentrations (Fig. 2b) returns a slope of 0.97, an offset of $4.9\,\mathrm{cm^{-3}}$ and an R^2 of 0.47. However, there is a substantial amount of scatter. Most notably, there is a cloud of data points below the 1:10 line ($\sim$ 7–8% of the data) that seems to be associated with colder temperatures at the sampling site (Fig. 2c).

Temperatures below 0°C could indicate the presence of ice crystals (e.g. in ice or mixed-phase clouds). Both the GCVI

240   and the FM-120 were calibrated using spherical particles, which makes the comparison especially difficult for cases when ice crystals are sampled. The true transmission efficiency of the GCVI inlet is going to be different for non-spherical particles, i.e. ice crystals, which are not accurately represented by glass beads. In addition, the concept of size becomes ambiguous when the sampled particles are not spherical, especially since the two instruments deal with different types of size. The optical size reported by the FM-120 is not necessarily the same as the Stokes equivalent size that determines how a crystal behaves inside

245   the GCVI inlet, which means that the transmission efficiency we apply could be incorrect. For non-spherical ice crystals, the sizing uncertainties in the fog monitor can be larger than those associated with Mie theory (Baumgardner et al., 2017), and as a result under- or oversizing of crystals can occur. This could also affect the concentration comparison. However, the points below the 1:10 line in Fig. 2 ($\sim$ 7–8% of the data) still remain below the 1:1 line even if we compare the cloud residual concentration to the total, uncorrected cloud particle concentration (not shown), which suggests that something other than

250   errors in the assumed transmission efficiency is causing the difference.

Riming or impaction scavenging of interstitial aerosol particles onto an ice crystal could result in more than one cloud residual emerging from the crystal as it dries inside the GCVI inlet (e.g., Mertes et al., 2007; Santachiara et al., 2018). Similarly,
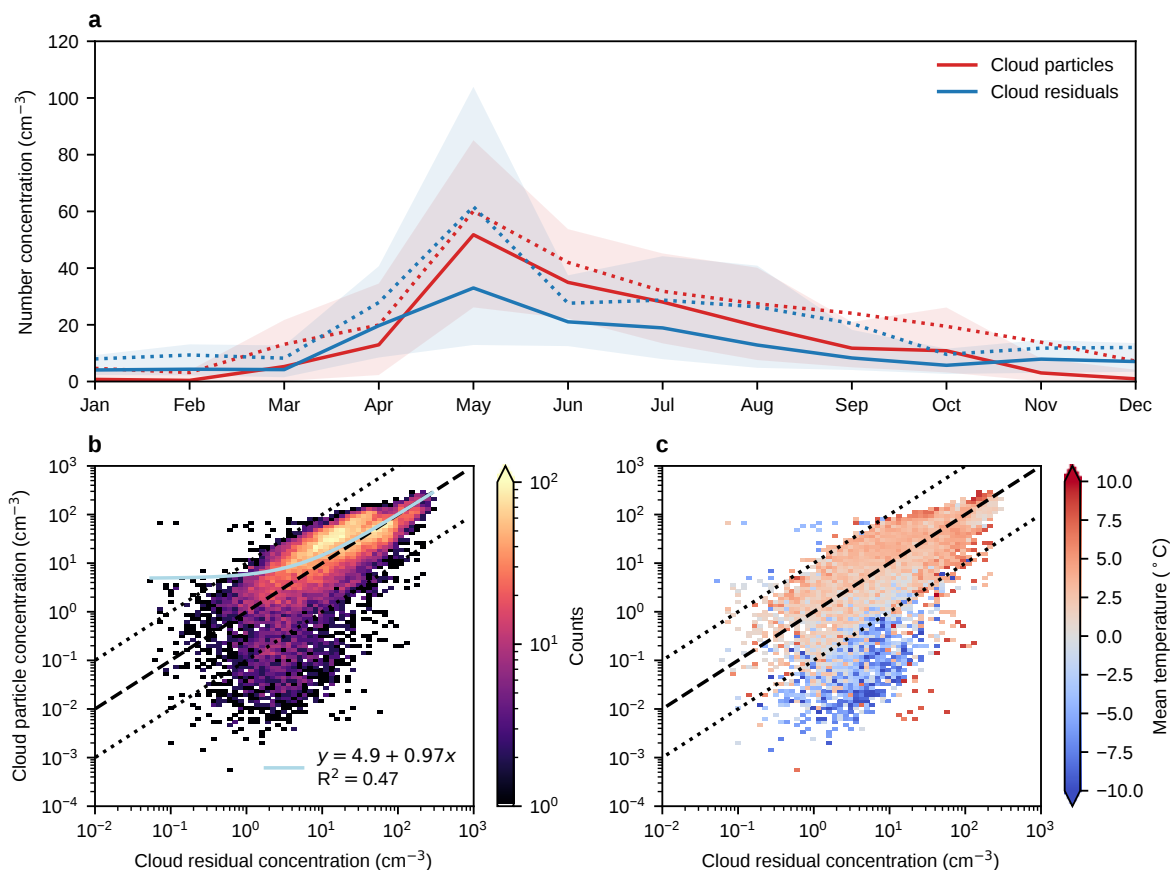
Figure 2. Comparison of cloud residual number concentrations and ambient cloud particle concentrations. a Monthly averages of cloud residual number concentrations as measured behind the GCVI (blue) and cloud particle number concentrations as measured by the FM-120 fog monitor (red). Solid and dotted lines show mean and median values, respectively, and shaded areas indicate the 25th to 75th percentile ranges. **b** Density scatterplot of cloud residual versus cloud particle number concentrations, including an orthogonal distance linear regression (grey line). **c** The same as b, but colourcoded by the average temperature instead of the data point density. In b and c, the black dashed line represents the 1:1 line and the dotted lines represent 10:1 and 1:10 lines. The transmission efficiency of the GCVI inlet (Shingler et al., 2012) has been included in the calculation of the cloud particle number concentration in all panels.

an INP could break or eject material during the freezing process (e.g., Lauber et al., 2018) which could also result in more than one residual particle per crystal. These processes could make cloud residual concentrations exceed cloud particle concentrations; however, the concentrations in Fig. 2 sometimes differ by almost two orders of magnitude, and it is unlikely that the aforementioned processes could account for the full difference (Santachiara et al., 2018).

Measurement artefacts during in-situ sampling of cloud droplets and ice crystals are a common and complex challenge (Baumgardner et al., 2017) contributing to both overestimation and underestimation of cloud residual (or cloud particle) con-

centration measurements (Pekour and Cziczo, 2011; Spiegel et al., 2012; Shingler et al., 2012). Particle capture by wake effects

260 in the GCVI inlet is a possible explanation for cloud residual concentrations exceeding cloud particle concentrations; however, even at cloud particle and interstitial aerosol particle concentrations at the upper end of our observed values, only 1 % of the measured cloud residuals is estimated to be a potential artefact (Pekour and Cziczo, 2011). Thus, this effect is likely not the major cause of the disparity between cloud residual and cloud particle concentrations that sometimes occurs. Droplet or ice crystal shattering is another potential source of small particles within the acceleration and deceleration zones of the GCVI, and

265 this could also cause an overestimation of the cloud residual number concentration. Intuitively, one would expect shattering events to produce large amounts of particles, yet the largest relative differences between cloud particle and cloud residual concentrations mainly occur at very low particle concentrations. Nevertheless, the apparent correlation with cold temperatures (Fig. 2c) means that ice crystal shattering inside the GCVI inlet cannot be fully ruled out.

A comparison of the measured visibility and the visibility calculated from the FM-120 data shows a reasonable agreement

270 for the majority of data points, but again there is a group of data points at predominantly cold temperatures where the agreement is much worse (Fig. S4a–b in supplementary material). The visibility was calculated using the Koschmieder formula (Seinfeld and Pandis, 2016), the measured cloud particle size distribution of the FM-120 and Mie theory (Python package *PyMieScatt* (v. 1.7.5); Sumlin et al., 2018) by assuming spherical particles with the refractive index of water (1.33) and a wavelength of 880 nm (of the visibility sensor). We have already suggested that the assumption of spherical particles might not hold at cold

275 temperatures, which could explain the differences in Fig. S4. However, the calculated visibility is sometimes several orders of magnitude higher than the measured one, and it seems unlikely that non-sphericity would cause such large differences. The presence of precipitating particles may cause the measured visibility to be higher than the calculated one; however, precipitating particle concentrations at Zeppelin Observatory have previously been found to be mostly lower than 0.3 cm^{-3} (Koike et al., 2019). Hence, while the presence of such particles could explain the differences in visibility, they do not explain the

280 differences in concentration in Fig. 2. Local effects of blowing snow could also affect the measured visibility, but there is no apparent correlation between wind speed and differences in cloud particle and cloud residual concentrations (see Fig. S5 in supplementary material). Thus, we are left with the possibility that the differences in visibility are caused by a loss of detected cloud particles within the FM-120. It could be that ice crystals are more susceptible to losses due to turbulent deposition inside the contraction of the inlet (Spiegel et al., 2012).

285 Recalculating the visibility after scaling up the cloud particle size distributions to the measured cloud residual concentrations (i.e. multiplying each cloud particle size distribution by the ratio of the total cloud residual concentration and the cloud particle concentration integrated above the GCVI cut-size) significantly improves the agreement with the measured visibility (see Fig. S4c–d in supplementary material). Note that the concentrations were only scaled up, not down, since the total cloud particle concentrations could be higher than the cloud residual concentrations due to the cut-size of the GCVI inlet. The

290 improvement in the visibility comparison after scaling the cloud particle concentrations points towards an undercounting of cloud particles in the FM-120 for parts of the period with colder temperatures. Thus, it cannot be ruled out that the discrepancy between the measured and calculated visibilities, and by extension the discrepancy between cloud residual and cloud particle concentrations, is partly due to the FM-120 undercounting the ambient ice crystals.

Atmospheric
Chemistry
and Physics
Discussions

As we have seen, interpreting cloud residual data is a non-trivial task. There are many processes, both natural and instrument

295 related, that can influence the measured concentrations of both cloud residuals and cloud particles. We cannot definitively say which sources of error are affecting which instrument, and therefore we will not discard any data at this stage. Still, a more detailed comparison with respect to temperature and wind parameters – also including data from the whole-air inlet – is warranted, and this is done in the next subsections.

In Fig. 2, we corrected the cloud particle concentrations for the GCVI transmission efficiency. However, to be able to compare

300 our cloud residual measurements to the aerosol particle measurements from the whole-air inlet, we need to apply the correction in the other direction. The integrated transmission efficiency of the GCVI inlet was estimated by calculating the ratio of the integrated cloud particle number concentrations with and without taking into account the size-dependent transmission efficiency of Shingler et al. (2012). Figure S6 shows the results when integrating over the entire cloud particle population and when integrating only above the cut-size diameter of the GCVI. Above the GCVI droplet/crystal cut-size (red histogram in

305 Fig. S6a), the distribution is symmetrical and relatively narrow, and it shows that approximately half (mean ± std ratio of 0.5 ± 0.05) of the total cloud particles were sampled. The mode of the distribution shows very little variation between seasons (Fig. S6b). We have therefore corrected all cloud residual size distributions and concentrations by a factor of 2 assuming cloud residual size and cloud particle size are not correlated. An individual correction factor for each data point would, in theory, be possible, but only for the points where we have overlapping cloud particle and cloud residual data. Thus, for the sake of

310 consistency, we use a constant correction factor.

3.1 Comparison with respect to ambient (acoustic) temperature

Figure 3 shows concurrent cloud particle, cloud residual and total aerosol particle data binned by ambient temperature (acoustic temperature recorded by the anemometer). Note that the acoustic temperature was, on average, 3.4°C higher than the actual air temperature (see Sect. 2.3.3) at Zeppelin Observatory during our measurement period. Panel a shows box plots of cloud

315 residual concentrations (corrected by the factor 2, see above) and cloud particle concentrations (now without correction, but still integrated only above the GCVI cut-size). The concentrations agree well down to about -2 to -4°C, where the cloud particle concentrations drop below the cloud residual concentrations. These bins contain relatively few data points (bar plot in Fig. 3a), but they follow the general trend of decreasing cloud particle/cloud residual concentrations with decreasing temperature.

Figure 3b shows the mean cloud residual and total aerosol particle size distributions for the same temperature bins. Both the

320 Aitken and the accumulation mode are present in both cloud residuals and total particles, but the total particle size distributions generally show higher particle concentrations, particularly of Aitken mode particles. Figure 3c shows the ratio between the distributions in panel b, i.e. cloud residual concentrations divided by total particle concentrations. At temperatures above approximately -2°C, the resulting curves are sigmoidal like typical CCN-activated particle fraction curves. During cloud events at these temperatures, the figure shows that most of the total aerosol particles larger ∼100 nm are in fact cloud residuals. The

325 apparent $D_{50\%}$, defined as the diameter where the ratio is around 0.5, decreases with decreasing temperature, which could be related to the general decrease in particle concentrations with temperature seen in the other two panels of the figure, since lower overall particle concentrations could allow smaller particles to activate (assuming liquid droplet activation without size-
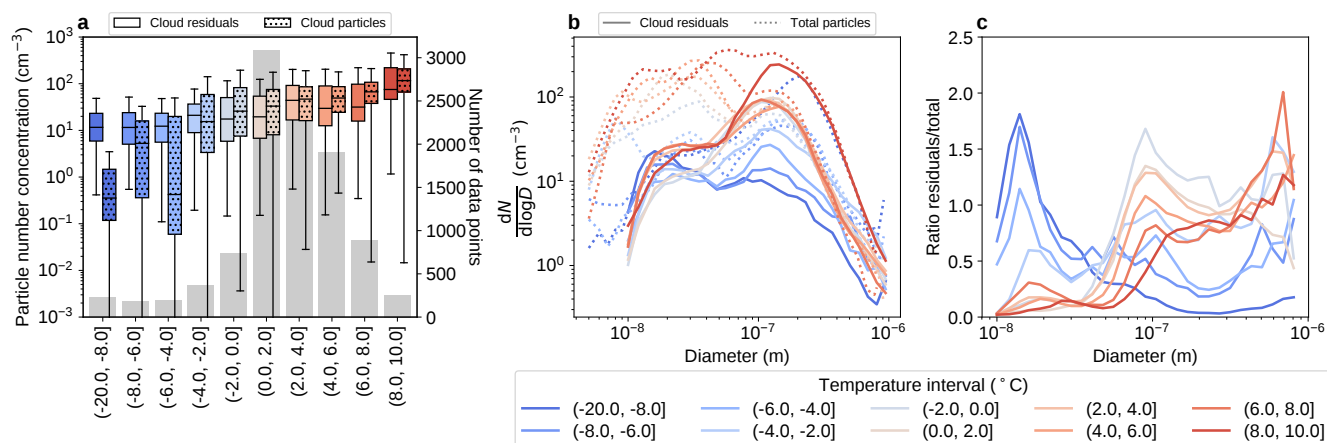
Figure 3. In-cloud data binned by temperature. a Box plot of cloud residual (solid) and cloud particle (hatched) number concentrations for different temperature intervals (see legend). Note that the temperature is the acoustic temperature measured by an anemometer. The grey bars in the background indicate the number of cloud residual data points (right y-axis) per temperature bin. **b** Mean particle number size distributions of cloud residuals (solid) and total particles (dotted) for different temperature intervals (see legend). **c** Ratio of the size distributions in b, i.e. cloud residual concentrations divided by total particle concentrations.

dependent chemical composition if the meteorological conditions are the same). Despite all the uncertainties and assumptions being made (e.g. CVI sampling efficiency and enrichment factor), it is encouraging to see that overall ratios are in the range

330 of expected values giving further faith in our observations. Ratios above 1 can be explained by the uncertainties in sampling efficiency and enrichment factor of the CVI system (see Sect. 3 above) and small uncertainties in sizing, concentration and losses of the DMPS.

At temperatures below -2°C (approximately 16 % of this subset of data), however, the curves in Fig. 3c look very different. Instead of an S-shape, the curves are relatively flatter with a maximum appearing at lower sizes, with the coldest temperature

335 bins even showing a peak below ∼20 nm particle diameter. This implies that accumulation mode particles have not acted as cloud residuals, while now an increased contribution of Aitken mode particles served as cloud seeds. These clouds most likely contain ice particles and the question arises if the small particles could potentially be caused by sampling artefacts inside the CVI sampling line (see Sect. 3 above) or if real physical atmospheric process is underlying this observation. While artefacts cannot be completely ruled out (see Sect. 3), it should be noted that approximately the same size modes are present in the

340 whole-air inlet (Fig. S7), and there is no reason to expect that any potential droplet or crystal shattering in this inlet should produce the same size particles as shattering in the GCVI inlet. The shape of the ratio curves in Fig. 3c below -2°C indicate the participation of ice in cloud formation as will be discussed in Sect. 5 within a cluster analysis of the residual size distributions.
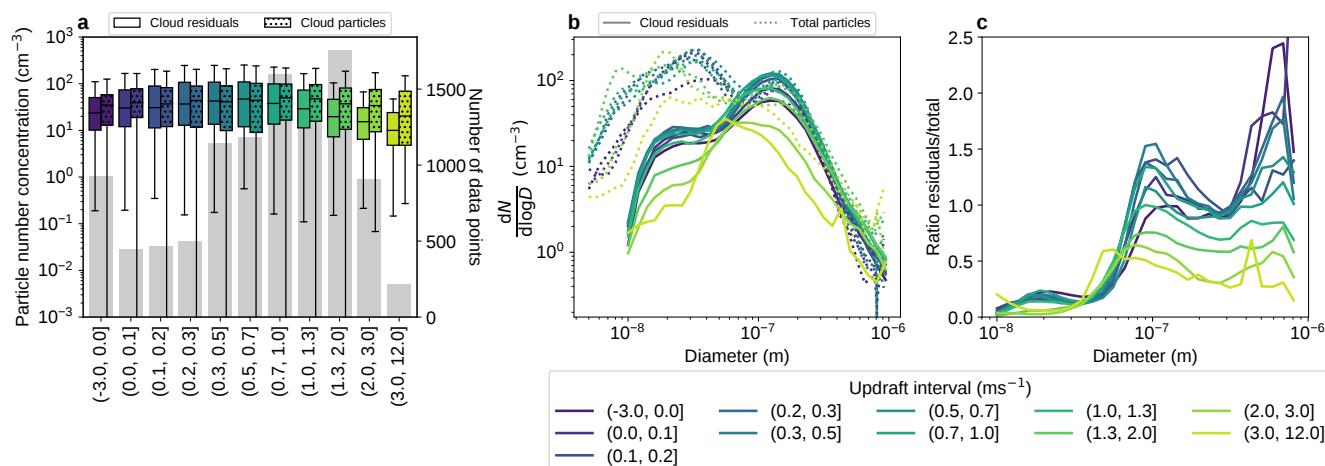
Figure 4. In-cloud data binned by updraft. a Box plot of cloud residual (solid) and cloud particle (hatched) number concentrations for different updraft intervals (see legend). The grey bars in the background indicate the number of cloud residual data points (right y-axis) per updraft bin. **b** Mean particle number size distributions of cloud residuals (solid) and total particles (dotted) for different updraft intervals (see legend). **c** Ratio of the size distributions in b, i.e. cloud residual concentrations divided by total particle concentrations.

3.2 Comparison with respect to updraft

The FM-120 as well as the GCVI inlet sampling efficiency can also be affected by the wind speed and direction (Spiegel et al.,
345   2012), but this is not something we can easily correct for. However, heatmaps similar to Fig. 2c for wind speed, updraft, and
wind direction indicate no obvious correlation between wind parameters and deviations of concentrations from the 1:1 line (see
Fig. S5). One should also take into account that high wind speeds are only rarely observed at Zeppelin Observatory (the median
wind speed is approximately $3\,\mathrm{ms^{-1}}$), which can be seen in Fig. S1. Nevertheless, since Zeppelin Observatory is a mountain
site, a closer look at the updraft is warranted to investigate potential orographic effects.

350   Figure 4 shows concurrent cloud particle, cloud residual and total aerosol particle data, this time binned by updraft veloc-
ity instead of acoustic temperature. The box plots in the first panel show that the cloud residual and cloud particle number
concentrations generally agree well, but there seems to be a tendency for the cloud residual number concentrations to be un-
derestimated at higher updraft, starting approximately above $1\,\mathrm{ms^{-1}}$. Panels b and c show a similar pattern, with cloud residual
concentrations decreasing in the last four updraft bins. This pattern is not observed in the total aerosol particles, except for in
355   the highest updraft bin (Fig. 4b). The curves in Fig. 4c systematically level out at lower ratios with higher updrafts (for the last
four bins), which could either mean that not all accumulation mode particles are cloud residuals under these conditions, or that
the GCVI inlet fails to sample all cloud particles at high updrafts. Taken together with the previous panels, it seems likely that
the GCVI inlet sampling efficiency is negatively affected by high updraft velocities (or indeed high wind speeds in general, as
these parameters tend to be correlated at Zeppelin Observatory). The sampling efficiency of the FM-120 fog monitor can in
360   theory also be adversely affected by high wind speeds (Spiegel et al., 2012), but this seems to happen to a lesser extent than

for the GCVI inlet based on Fig. 4a. One should bear in mind that the wind speeds and updrafts are generally lower near the FM-120 as it is positioned at a lower altitude than the GCVI inlet ($\sim$5 m below).

4 The annual cycle of Arctic cloud residuals at Zeppelin Observatory

During cloud events within our measurement period, typical cloud residual number concentrations ranged between 10 and 62 cm^{-3} (25$^{\text{th}}$ and 75$^{\text{th}}$ percentiles), with a median of 25 cm^{-3} (mean $\pm$ standard deviation: 50 ± 66 cm^{-3}). Total concentrations of particles suspended in the air (diameters 10–809 nm) during these cloud events were generally higher, ranging up to 163 cm^{-3} (75$^{\text{th}}$ percentile) with a median of 70 cm^{-3} (mean $\pm$ standard deviation: 145 ± 235 cm^{-3}).
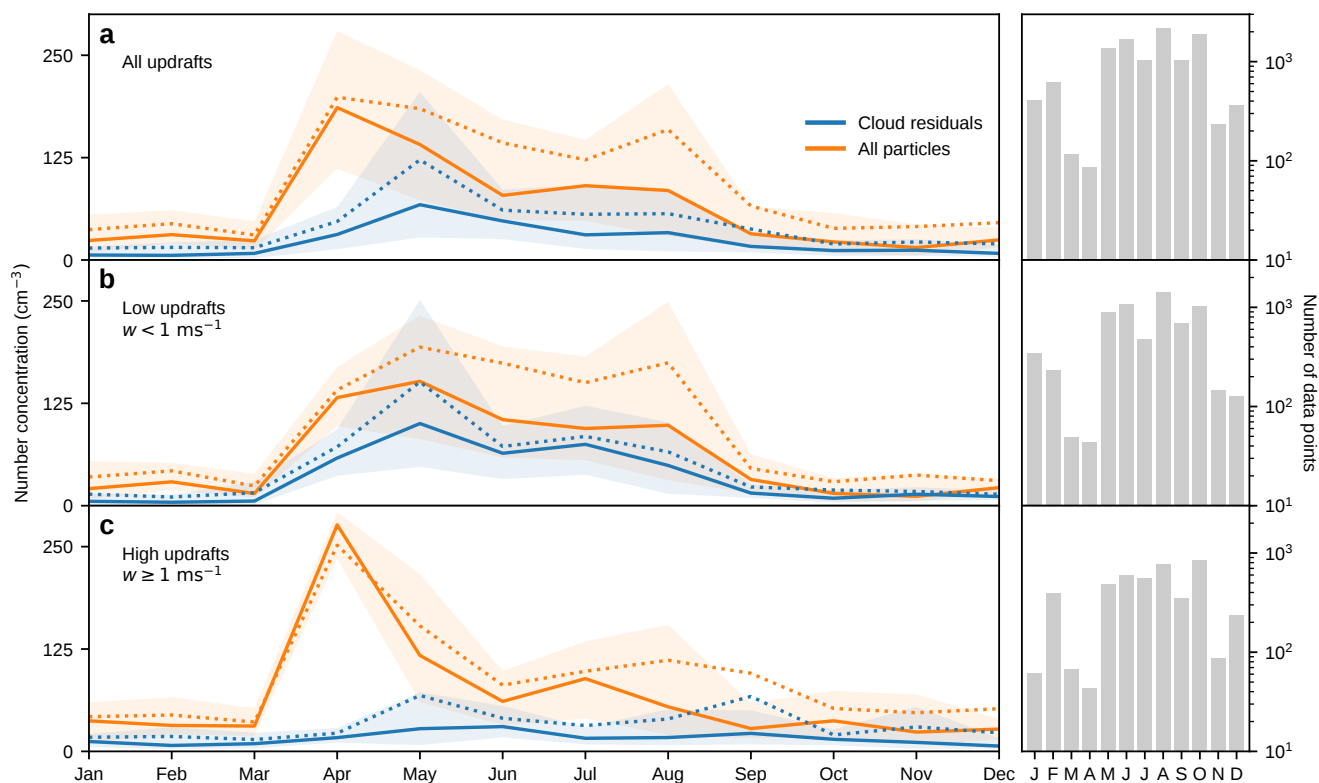
Figure 5. Annual cycle of total and cloud residual number concentrations. Monthly averages of total (orange) and residual (blue) particle number concentrations integrated above 20 nm, measured at Zeppelin Observatory, Svalbard during the period Nov 2015–Feb 2018. Solid and dotted lines show median and mean values, respectively, and shaded areas indicate the 25$^{\text{th}}$ to 75$^{\text{th}}$ percentile ranges. Data have been segregated based on the updraft velocity at the station, w. The panels show data for **a** all w, **b** $w < 1$ ms^{-1}, **c** $w \geq 1$ ms^{-1}, and the corresponding bar charts show the number of data points per month.

15

Atmospheric
Chemistry
and Physics
Discussions

Figure 5 shows concurrent monthly averages of total particle and cloud residual number concentrations above 20 nm diame-
ter. Panel a shows all data, whereas panels b and c show data for updraft velocities below and above $1 \, \mathrm{ms}^{-1}$, respectively. This
370 boundary was chosen partly based on Fig. 4, but also because updraft velocities in marine stratiform clouds are typically below
$1 \, \mathrm{ms}^{-1}$ (Zheng et al., 2016) and hence higher updraft velocities could be indicative of orographic effects at the station. The bar
charts next to each panel indicate the number of data points per month.

The observed total particle number concentrations follow the typical seasonal cycle of Arctic aerosol. We recognise the
characteristic maxima in number concentration due to Arctic haze in spring and new particle formation in summer, and the
375 low, relatively stable concentrations during the rest of the year. There are some differences compared to previous measurements
at Zeppelin Observatory, for example in terms of when peak concentrations occur (e.g., Ström et al., 2003; Tunved et al., 2013;
Freud et al., 2017). Such differences could be due to annual variability, which has previously been shown to be significant
(Freud et al., 2017). In addition, it should also be kept in mind that we present number concentrations exclusively during cloud
events and concentrations shown are for particles above 20 nm diameter, in contrast to previous studies.

380 The cloud residual number concentrations, while lower than the total particle concentrations, display a similar seasonal
behaviour. The shape and the magnitude of the cloud residual annual cycle are confirmed by ambient cloud particle measure-
ments (cf. Fig. 2a). Based on Fig. 5a, the springtime peak in cloud residual concentrations appears to lag that of the total aerosol
particles by one month – the maximum cloud residual concentration occurs in May rather than in April. However, this apparent
shift does not appear if we only consider low updraft cases (Fig. 5b). The total particle concentration peak in April in Fig. 5a
385 appears to be driven by the high total particle number concentrations in April during high updraft events (Fig. 5c). Most of
the April data points in Fig. 5c are from the same event – a relatively thin cloud where a large difference between the cloud
residual and total particle concentrations was observed. Overall, the high updraft cases are characterised by very low cloud
residual number concentrations and the shape of the annual cycle is slightly different from the other two panels. This may
indicate that an explanation could be the potential decrease in the GCVI sampling efficiency at high updrafts (see Sect. 3.2).
390 One should also bear in mind that the months of March and April are characterised by a low number of observations (80-100
size distribution scans), limiting the statistical significance for these months for the concurrent data.

In terms of number size distribution (see Fig. 6), the cloud residual population is dominated by accumulation mode particles
during most of the year. However, the Aitken mode is often also present, and there appears to be a clear seasonality in the
relative abundance of Aitken and accumulation mode cloud residuals. In January and February, the median size distributions
395 are dominated by the Aitken mode. In spring, particularly April and May, there are very few Aitken mode cloud residuals in
comparison to the number of accumulation mode residuals. The size distributions then become more bimodal during summer
and autumn, then in December the Aitken mode dominates again. The size distributions in Fig. 6 are normalised to highlight
their shape. Non-normalised monthly cloud residual size distributions, together with concurrent total aerosol size distributions,
can be found in Fig. S8 in the supplementary material. Note, however, that the figures show different subsets of the data – Fig. 6
400 shows all cloud residual data we have, while Fig. S8 is limited by the availability of concurrent data from the whole-air inlet.
Generally speaking, the total aerosol size distributions and the cloud residual size distributions show similar size modes, but
the total aerosol concentrations are higher, particularly for the Aitken mode.

In Fig. 4, clear changes in the size cloud residual distributions (i.e. shift towards smaller activation diameters) are only seen for updrafts above around 2 ms^{-1}, which is a relatively small subset of the observations. The overall shape of the monthly

405 averaged cloud residual size distributions do not change significantly if only taking into account cases with updrafts below 1 ms^{-1} (see Fig. S9 in the supplementary material). As such, we will use all size distributions for all updrafts from now on.

5 The importance of Aitken mode particles in Arctic clouds

Figure 6 shows that Aitken mode cloud residuals, even below 30 nm in diameter, occur throughout the year at Zeppelin Observatory. In this size range, particles are often not considered to be potential CCN (nor INP), but a closer look at our measured

410 cloud residual size distributions shows that Aitken mode particles often make up a significant part of the total cloud residual number concentration. Figure 7 shows the seasonality of the contribution of sub-100 nm, sub-50 nm and sub-25 nm particles to the overall measured cloud residual population. The sub-100 nm size range is included for illustrative purposes, since 100 nm is sometimes used as a lower size threshold for particles to be considered CCN-active for liquid clouds (Kuang et al., 2009; Yu et al., 2014; Patoulias et al., 2015). The fractions presented in Fig. 7 have been calculated based on daily mean cloud residual

415 concentrations and show that particles smaller than 100 nm in diameter make up between 30 and 70 % of the total measured cloud residual number concentration in the majority of the cases. In fact, the average contribution (both mean and median) is close to or above 50 % in all but four months. The months where the sub-100 nm cloud residuals make up a smaller fraction of the total are the months when the total aerosol particle number concentration is the highest (April through July; cf. Fig. 5).

The seasonal pattern looks similar for all three cloud residual size ranges in Fig. 7. The relative contribution of Aitken mode

420 particles to the total cloud residual number concentration increases during autumn and continues to do so until it reaches a maximum in February. Then, when the haze period starts in March and April, the contribution of Aitken mode particles begins to decrease as the number of accumulation mode particles increases. The relative contribution of sub-100 nm particles is at its lowest in April, while the sub-50 nm and sub-25 nm relative contributions continue to decrease until June. This behaviour is opposite to the total aerosol particles, where the summer months are the months with the highest relative contribution of Aitken

425 mode particles due to the increased contribution of new particle formation (cf. Fig. S10).

To find out under which conditions the smaller residuals are present in the cloud particles, we performed k-means clustering on the cloud residual number size distributions (normalised by the corresponding total cloud residual number concentration). The results when 5 clusters are used are presented in Fig. 8. The clusters are numbered from 1 to 5 according to increasing modal diameters of the cluster average size distributions (the approximate modal diameters are 15, 30, 65, 100, and 150 nm).

430 This order is also reflected in the total number concentration (cf. Fig. S11). Cluster 2 is the most frequent cluster (27 % of the time) spread throughout the year but less in spring and early summer. This is followed by Clusters 5 and 4 (26 % and 25 %, respectively) which are more dominant in spring and summer. Cluster 3 (14 % of the time) occurs more in late summer and autumn, while Cluster 1 is the least frequent (8 % of the time) and occurs mostly during winter.

Two of the clusters (1 and 2 in Fig. 8) show cloud residual size distributions dominated by Aitken mode particles. The

435 accumulation mode Clusters (3, 4, and 5) show almost identical cloud particle number size distributions with a mode around
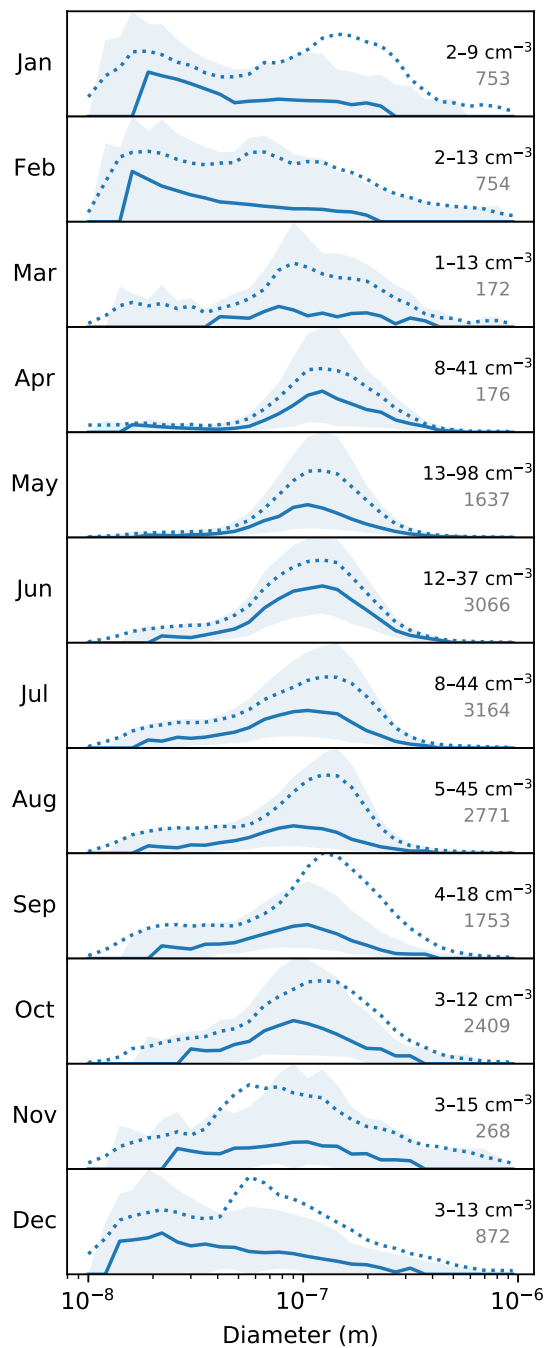
Figure 6. Monthly average cloud residual number size distributions. Solid and dotted lines show median and mean values, respectively, and shaded areas indicate the 25th to 75th percentile ranges. The numbers in the upper right corner of each panel indicates the 25th to 75th percentile ranges of the integrated number concentrations. The grey numbers below indicate the number of data points we have per month. Concurrent cloud residual and whole-air size distributions are shown for comparison in Fig. S8 in the supplementary material.
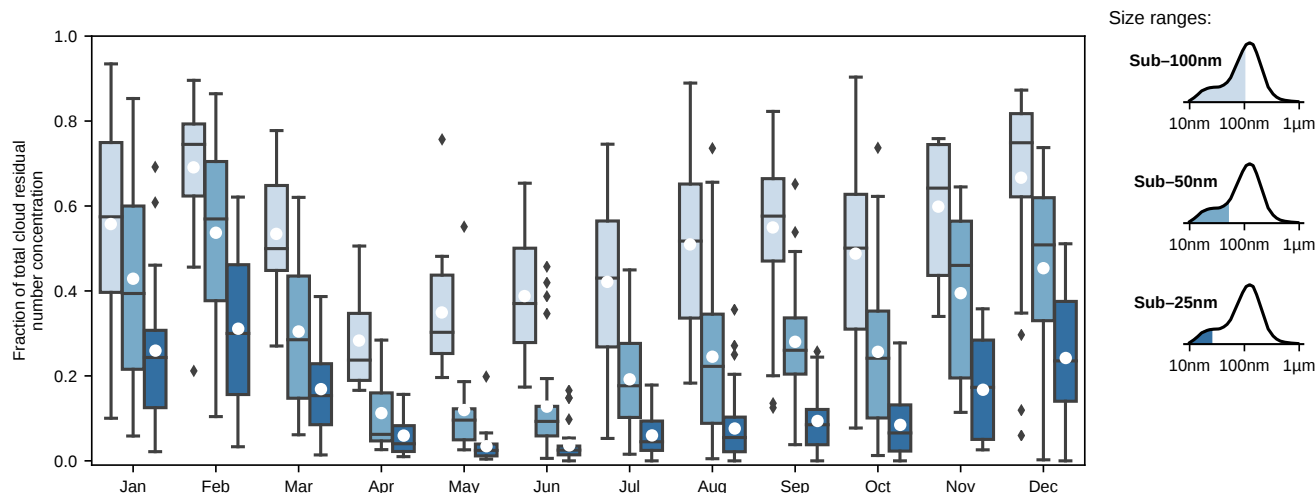
Figure 7. Contribution of small particles to the overall cloud residual population. Box plot of daily average contributions (fraction of the total cloud residual number concentration) of Aitken mode particles to the cloud residual population. The whiskers extend no more than 1.5 times the interquartile range past the edges of the box, and data points outside that range are marked by black diamonds. Mean values are indicated by white dots. The different shades of blue indicate the cloud residual size ranges sub-100 nm, sub-50 nm and sub-25 nm diameter (see legend).

12 μm cloud particle diameter. The Aitken mode clusters, on the other hand, are associated with larger cloud particles (Fig. 8a) and the lowest cloud particle and cloud residual number concentrations (Fig. S11), suggesting they represent optically thin clouds with few, large droplets and/or ice crystals. This is further corroborated by the visibility distribution (Fig. S11) which shows high values, in particular for Cluster 1. Cluster 1 also stands out in that it occurs primarily during the winter months and
440 at low temperatures (Fig. S11). No clear relationship between these two clusters and wind speed or updraft was found.

The ratio between cluster mean cloud residual size distributions and corresponding mean ambient particle size distributions, for liquid clouds this would correspond to the activation ratio, are shown in Fig. S7 in the supplementary material. Cluster 1 and (to a lesser degree) Cluster 2 clearly deviate from the classical Köhler theory of droplet activation assuming a size-independent chemical composition. It is possible that differences in particle composition could explain part of this behaviour
445 (e.g., McFiggans et al., 2006; Lowe et al., 2019); however, liquid droplet activation is not the only relevant process at our site and therefore the cloud residual distributions we measure could also be related to ice processes. The fact that Cluster 1 occurs predominantly during winter and at lower temperatures than the other clusters (Fig. S11) would also be consistent with an influence from ice processes.

Comparing the target classification of Cloudnet above Ny-Ålesund, at the altitude around Zeppelin Observatory, to the
450 cluster analysis indeed shows a higher occurrence of ice for Cluster 1 (Fig. 9 and Fig. S12a in supplementary material). Note that the Cloudnet comparison could only be made for a subset of the data (see Sect. 2.3.4), but the relative cluster occurrence in this subset is similar to that in the full dataset. Interestingly, the ratio of ice to liquid occurrence (Cloudnet category 4 divided
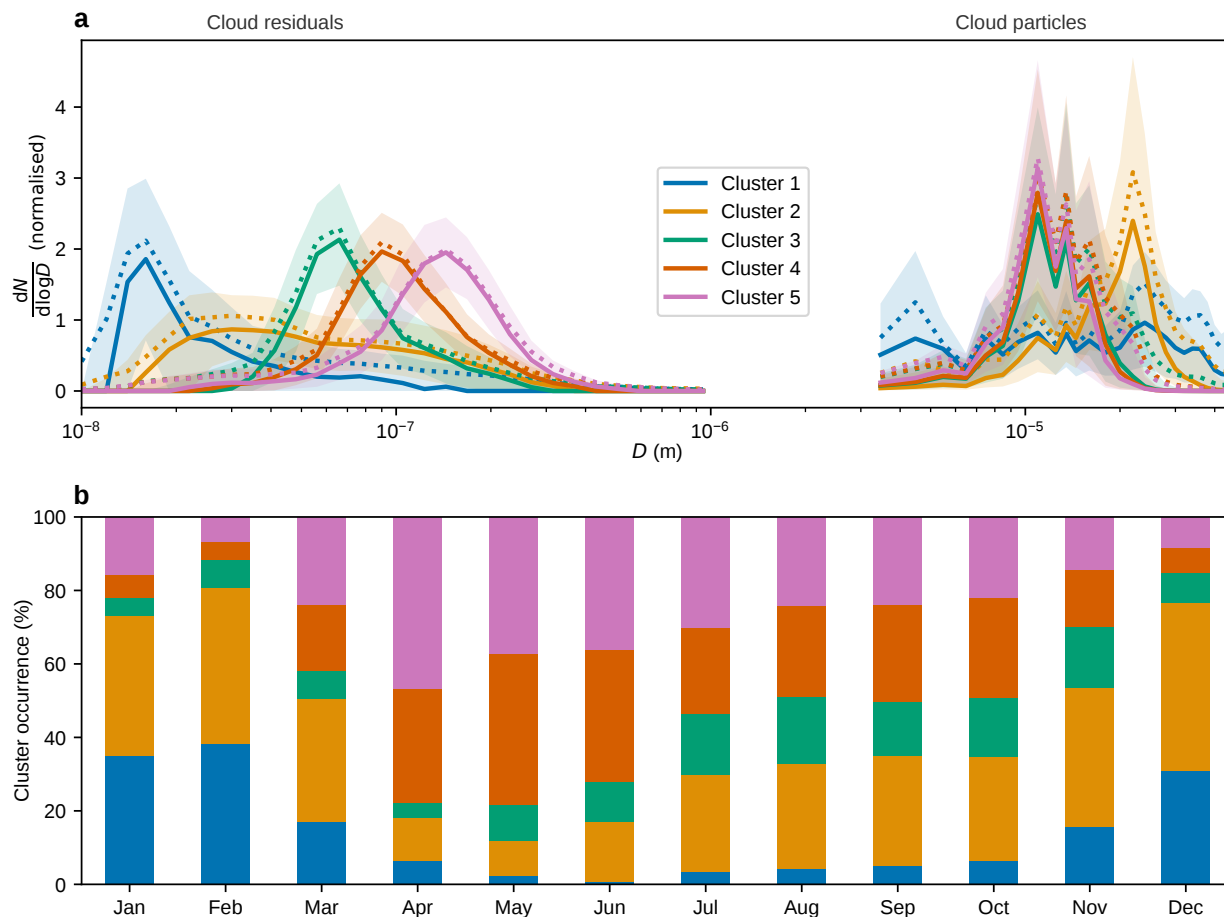
Atmospheric
Chemistry
and Physics
Discussions
Open Access
EGU

Figure 8. Results of k-means clustering of cloud residual number size distributions using 5 clusters. **a** Normalised cloud residual number size distributions for each cluster (left), and normalised number size distributions for the corresponding ambient cloud particle population (right). Solid and dotted lines show median and mean values, respectively, and shaded areas indicate the 25th to 75th percentile ranges. **b** Monthly frequency of occurrence of each cluster. Additional parameters (e.g. integrated cloud residual and cloud particle number concentrations, non-normalised cloud residual size distributions, etc.) for each cluster can be found in the supplementary material.

by category 1) decreases from Cluster 1 to Cluster 5, which is consistent with the activation ratios in Fig. S7 which appear more like classical Köhler activation (of homogeneously mixed particles) when moving from Cluster 1 to Cluster 5. However, it should be noted that all Cloudnet classification categories appear in each of the clusters (Fig. S12), so the cloud residual size distribution shapes cannot be solely attributed to one cloud particle type.
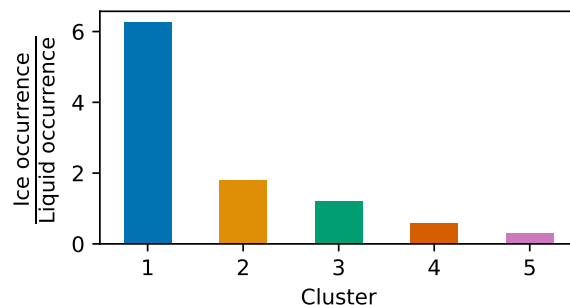
Figure 9. Ratio of ice to liquid occurrence per cluster based on Cloudnet retrieval. The bar chart shows, for each cloud residual size distribution cluster, the average ratio of pure ice to pure liquid occurrence, i.e. Cloudnet category 4 divided by Cloudnet category 1, around the altitude of Zeppelin Observatory. See Fig. S12 for a more detailed view on the average Cloudnet retrieval target classifications for each cluster.

6 Discussion

Results presented in this paper are the first direct long-term measurements of size resolved cloud residual number concentrations of low-level clouds in the Arctic. It is also the first cloud residual dataset that covers more than a full annual cycle, in the Arctic and globally. It includes the important winter months, when Arctic warming is most pronounced (Maturilli and Kayser, 2017) and clouds are hypothesised to play a key role. Our measured cloud residual number concentrations generally follow the typical annual aerosol cycle previously reported for this site (Tunved et al., 2013). During the autumn and winter months, we found, in relative terms, a significant contribution of Aitken mode particles to the cloud residual number concentration.

Cloud residual measurements differ from standard CCN measurements in that instead of attempting to replicate in-cloud conditions inside the instrument – most notably fixed supersaturation bands in place of dynamic ambient conditions – we extract cloud particles from the air, dry them and subsequently count and size the cloud residuals. While there are only a few long-term datasets from the Arctic (Jung et al., 2018; Dall'Osto et al., 2017; Schmale et al., 2018) that we can compare to, this difference in measurement techniques seems to be important. Jung et al. (2018) found that CCN concentrations correlated well with concentrations of accumulation mode particles at Zeppelin Observatory, and that median CCN concentrations peaked in March at most supersaturation levels. This is different from our measured cloud residual concentrations, which peak in May. However, one should keep in mind that Jung et al. (2018) considered different years (2007–2013) and did not differentiate between in- or out-of-cloud periods. In addition, Jung et al. (2018) observed for most of the year higher CCN concentrations than our cloud residual concentrations, particularly in winter, highlighting the differences between measurement techniques. Studies where particles are artificially activated, i.e. at a fixed supersaturation, are independent of the ambient meteorology and atmospheric dynamics, whereas our study inherently takes the ambient conditions into account by sampling the actual ambient cloud droplets or ice crystals. Therefore, the differences between our observed concentrations could either be because

the actual ambient supersaturations are lower than what is used in CCN counters, or because ice processes are involved while CCN counters only consider liquid droplet activation.

The importance of Aitken mode particles for Arctic clouds has previously been shown (e.g., Leaitch et al., 2016; Koike et al., 2019; Korhonen et al., 2008), however, by indirect means or model studies. Our results support these findings with direct measurements of cloud residuals. Furthermore, we find that Aitken mode particles also play an important role in wintertime clouds at Zeppelin Observatory, while previous observations have focused on the Arctic summer months. The clear seasonality we observe in the relative contribution of small particles to the cloud residual number concentration could partly be explained by the interplay between aerosol particle sources, sinks, meteorology and condensible water vapour. In late autumn and winter, aerosol particle concentrations decrease rapidly (Fig. 5) and the Arctic atmosphere becomes drier (Maturilli and Kayser, 2017). However, if the decrease in condensation sink, due to reduced particle concentration, is larger than the decrease in water vapour, there will be, in relative terms, more water vapour available for fewer particles in winter. These conditions allow for higher supersaturation to be reached and smaller particles to be activated (assuming no strong seasonal cycle in the updraft velocity as observed here, see Fig. S1). In other words, the winter season at Zeppelin Observatory falls into the CCN-limited cloud–aerosol regime that has previously been reported for the summertime High Arctic (Mauritsen et al., 2011; Leaitch et al., 2016). However, this only applies to liquid clouds, while the cloud residuals we measure could correspond to either CCN or INP. Unfortunately, no cloud phase data are available for our measurement period but, by proxy of the Cloudnet target classification from above Ny-Ålesund, we have shown that the cloud residual size distributions dominated by the very smallest particles are likely to be influenced by ice processes.

Some of the cloud residuals we have measured, in particular those in Clusters 1 and 2, are much smaller than typical INP (Hoose and Möhler, 2012; DeMott et al., 2010) (or indeed CCN). Yet residual size distributions with a similar shape have previously been observed for ice particles in mixed-phase clouds measured with an Ice-CVI (Mertes et al., 2007), and droplet residuals down to 25 nm diameter have previously been observed by GCVI measurements (Schwarzenboeck et al., 2000) and predicted in model studies (Gérémy et al., 2000; Korhonen et al., 2008).

A question that arises is where these small particles come from. In the Arctic and marine boundary layer, the presence of particles below ∼50 nm is most often associated with new particle formation (Ström et al., 2003; Tunved et al., 2013) or primary emissions of sea spray particles (Ovadnevaite et al., 2011). However, these sources are unlikely to explain the presence of small particles during winter, when there is reduced or no sunlight (i.e. no photochemistry), less biological production and most of the sea surface is covered by ice (Dall'Osto et al., 2017; Sharma et al., 2012). Other potential sources can be long-range transport, but the lifetime of Aitken mode aerosol particles in the boundary layer is rather limited, or entrainment from the free troposphere. However, this is purely speculative and future studies are needed to investigate the exact sources and chemical nature of these small particles.

As the remote-sensing results suggest, the ice phase appears at the height of Zeppelin Observatory predominantly during mixed-phase cloud conditions. It could potentially be that the crystals we measure are the result of secondary ice formation processes (Field et al., 2016), which has been suggested in a model study to be important for Arctic stratocumulus clouds (Sotiropoulou et al., 2020). This could include a distribution of the original CCN or INP material to the ice splinters, which act

as new nuclei to further ice particle formation. In other words, the cloud residuals we measure do not have to correspond to single CCN or INP but may also be fragments of these which would explain their small size. The shape of the cloud residual size distribution of Cluster 1 compared to the ambient particle size distribution (cf. Fig. S7a) reveals that the accumulation mode

515   particles do not activate. This points towards a possible water vapour transfer to the ice splinters via the Bergeron–Findeisen process causing a larger concentration of interstitial aerosol particles. However, it should be noted that secondary ice particles cannot be the only reason for the small residuals we observe, as it would not explain why the cloud residual and cloud particle concentrations do not always agree during these cases (see e.g. Fig. 3a) (unless the ice crystals are undersampled by the fog monitor, see Sect. 3). There are other processes, such as riming, which could be consistent with both small residuals and a

520   discrepancy between cloud residual and cloud particle concentrations. Additionally, since mixed-phase clouds are concerned, part of the cloud residuals will of course also come from liquid cloud droplets. It is not possible to tell if a given cloud residual is a result of liquid droplet activation (CCN), ice nucleation (INP), or secondary processes (CCN/INP fragment) without further detailed information on cloud phase, structure and origin. The cloud phase is an important parameter should as such be added in future studies.

525   Although an overall good agreement between ambient cloud particle and cloud residual number concentrations is found, one has to keep in mind that measurement artefacts can still not be fully excluded given the complexity of our observations. The initial data set was carefully screened for malfunctioning of instrumentation and local contamination. A thorough assessment of potential artefacts and instrument uncertainties was made in Sect. 3. While there were some cases where the agreement between the GCVI and the FM-120 was clearly worse, we did not discard these data because we were unable to prove that the

530   disagreement was only caused by artefacts in the GCVI. In addition, the disagreement is not completely random – data points at cold temperatures are overrepresented (see Figs. 2 and S4). Thus, removing these points would have introduced a (potentially unjustified) bias into our analysis. Despite the uncertainties, we believe that our results are reliable enough to show that small particles are likely contributing to the formation of mixed-phased clouds at Zeppelin Observatory. This is especially important during the dark period when overall aerosol concentrations are low and even small changes in available CCN and INP will

535   have a strong impact on cloud properties.

7   Conclusions

Our study presents a unique seasonal picture of aerosol particle activation in clouds in a polar environment and is the first long-term study of cloud residuals in the Arctic. Activation of aerosol particles in low-level clouds in the Arctic is strongly coupled to the annual variability of aerosol particle number and size distribution, meteorology and the availability of water vapour. We

540   have demonstrated that the use of CCN proxies with fixed size limits (e.g. 100 nm diameter) or accumulation mode aerosol particles is incorrect for the Arctic environment, where smaller particles act as CCN, supporting the results of previous studies. For large parts of the year, and especially during the dark period, we observed a large relative contribution of Aitken mode particles to the cloud residuals, which could be explained either by a strong CCN-limited regime or ice processes, possibly including secondary ice formation. In winter, the Arctic exhibits the strongest warming trend and clouds are believed to play

545   an important role in this process. Even subtle changes in aerosol particle number concentrations during the dark period in the Arctic can result in large effects on cloud microphyscial properties and thus also perturb cloud-related warming effects by changing the radiation balance in the infrared spectrum. The climatology presented here provides a new benchmark dataset for further model–measurement evaluation exercises to improve the representation of low-level clouds in Earth system models. Our work also shows the importance of focusing more research in the Arctic on the dark period. We have demonstrated the

550   experimental complexity involved in aerosol-cloud interaction research, highlighting the strengths and weaknesses of sampling cloud droplets and crystals by means of the GCVI technique. The direct measurements of cloud residuals provide a valuable new perspective on Arctic CCN and INP, but information about the cloud particle phase and the residual chemical composition would be necessary to be able to disentangle and better understand all the processes and particle sources involved in Arctic cloud formation.

References

575 Baumgardner, D., Abel, S. J., Axisa, D., Cotton, R., Crosier, J., Field, P., Gurganus, C., Heymsfield, A., Korolev, A., Krämer, M., Lawson, P., McFarquhar, G., Ulanowski, Z., and Um, J.: Cloud Ice Properties: In Situ Measurement Challenges, Meteor. Monogr., 58, 9.1–9.23, https://doi.org/10.1175/AMSMONOGRAPHS-D-16-0011.1, 2017.

Boucher, O., Randall, D., Artaxo, P., Bretherton, C., Feingold, G., Forster, P., Kerminen, V.-M., Kondo, Y., Liao, H., Lohmann, U., Rasch, P., Satheesh, S., Sherwood, S., Stevens, B., and Zhang, X.: Clouds and Aerosols, in: Climate Change 2013 - The Physical Science Basis.

580 Contribution of Working Group I to the Fifth Assessment Report of the Intergovernmental Panel on Climate Change, edited by Stocker, T., Qin, D., Plattner, G.-K., Tignor, M., Allen, S., Boschung, J., Nauels, A., Xia, Y., Bex, V., and Midgley, P., pp. 571–658, Cambridge University Press, Cambridge, United Kingdom and New York, NY, USA, https://doi.org/10.1017/CBO9781107415324.016, 2013.

Dahlke, S. and Maturilli, M.: Contribution of Atmospheric Advection to the Amplified Winter Warming in the Arctic North Atlantic Region, Advances in Meteorology, 2017, 1–8, https://doi.org/10.1155/2017/4928620, 2017.

585 Dall'Osto, M., Beddows, D. C., Tunved, P., Krejci, R., Ström, J., Hansson, H. C., Yoon, Y. J., Park, K. T., Becagli, S., Udisti, R., Onasch, T., Ódowd, C. D., Simó, R., and Harrison, R. M.: Arctic sea ice melt leads to atmospheric new particle formation, Scientific Reports, 7, 1–10, https://doi.org/10.1038/s41598-017-03328-1, 2017.

DeMott, P. J., Prenni, A. J., Liu, X., Kreidenweis, S. M., Petters, M. D., Twohy, C. H., Richardson, M. S., Eidhammer, T., and Rogers, D. C.: Predicting global atmospheric ice nuclei distributions and their impacts on climate, Proceedings of the National Academy of Sciences,

590 107, 11 217–11 222, https://doi.org/10.1073/pnas.0910818107, 2010.

Ebell, K., Nomokonova, T., Maturilli, M., and Ritter, C.: Radiative Effect of Clouds at Ny-Ålesund, Svalbard, as Inferred from Ground-Based Remote Sensing Observations, Journal of Applied Meteorology and Climatology, 59, 3–22, https://doi.org/10.1175/JAMC-D-19-0080.1, 2020.

Field, P. R., Lawson, R. P., Brown, P. R. A., Lloyd, G., Westbrook, C., Moisseev, D., Miltenberger, A., Nenes, A., Blyth, A., Choular-

595 ton, T., Connolly, P., Buehl, J., Crosier, J., Cui, Z., Dearden, C., DeMott, P., Flossmann, A., Heymsfield, A., Huang, Y., Kalesse, H., Kanji, Z. A., Korolev, A., Kirchgaessner, A., Lasher-Trapp, S., Leisner, T., McFarquhar, G., Phillips, V., Stith, J., and Sullivan, S.: Chapter 7. Secondary Ice Production - current state of the science and recommendations for the future, Meteor. Monogr., 58, 7.1–7.20, https://doi.org/10.1175/AMSMONOGRAPHS-D-16-0014.1, 2016.

Freud, E., Krejci, R., Tunved, P., Leaitch, R., Nguyen, Q. T., Massling, A., Skov, H., and Barrie, L.: Pan-Arctic aerosol number size distribu-

600 tions: Seasonality and transport patterns, Atmos. Chem. Phys., 17, 8101–8128, https://doi.org/10.5194/acp-17-8101-2017, 2017.

Gérémy, G., Wobrock, W., Flossmann, A. I., Schwarzenböck, A., and Mertes, S.: A modelling study on the activation of small Aitken-mode aerosol particles during CIME 97, Tellus B: Chemical and Physical Meteorology, 52, 959–979, https://doi.org/10.3402/tellusb.v52i3.17078, 2000.

Gierens, R., Kneifel, S., Shupe, M. D., Ebell, K., Maturilli, M., and Löhnert, U.: Low-level mixed-phase clouds in a complex Arctic environ-

605 ment, Atmos. Chem. Phys., 20, 3459–3481, https://doi.org/10.5194/acp-20-3459-2020, 2020.

Hoose, C. and Möhler, O.: Heterogeneous ice nucleation on atmospheric aerosols: a review of results from laboratory experiments, Atmos. Chem. Phys., 12, 9817–9854, https://doi.org/10.5194/acp-12-9817-2012, 2012.

Illingworth, A. J., Hogan, R. J., O'Connor, E. J., Bouniol, D., Brooks, M. E., Delanoë, J., Donovan, D. P., Eastment, J. D., Gaussiat, N., Goddard, J. W., Haeffelin, M., Klein Baltink, H., Krasnov, O. A., Pelon, J., Piriou, J. M., Protat, A., Russchenberg, H. W., Seifert, A., Tomp-

610 kins, A. M., van Zadelhoff, G. J., Vinit, F., Willen, U., Wilson, D. R., and Wrench, C. L.: Cloudnet: Continuous evaluation of cloud profiles

in seven operational models using ground-based observations, Bull. Amer. Meteor. Soc., 88, 883–898, https://doi.org/10.1175/BAMS-88-6-883, 2007.

Irish, V. E., Hanna, S. J., Willis, M. D., China, S., Thomas, J. L., Wentzell, J. J., Cirisan, A., Si, M., Leaitch, W. R., Murphy, J. G., Abbatt, J. P., Laskin, A., Girard, E., and Bertram, A. K.: Ice nucleating particles in the marine boundary layer in the Canadian Arctic during
615   summer 2014, Atmos. Chem. Phys., 19, 1027–1039, https://doi.org/10.5194/acp-19-1027-2019, 2019.

Jung, C. H., Yoon, Y. J., Kang, H. J., Gim, Y., Lee, B. Y., Ström, J., Krejci, R., and Tunved, P.: The seasonal characteristics of cloud condensation nuclei (CCN) in the arctic lower troposphere, Tellus B: Chemical and Physical Meteorology, 70, 1513 291, https://doi.org/10.1080/16000889.2018.1513291, 2018.

Kazadzis, S.: WMO/GAW Aerosol Measurement Procedures, Guidelines and Recommendations, Tech. rep., World Meteorological Organi-
620   zation, 2016.

Koike, M., Ukita, J., Ström, J., Tunved, P., Shiobara, M., Vitale, V., Lupi, A., Baumgardner, D., Ritter, C., Hermansen, O., Yamada, K., and Pedersen, C. A.: Year-Round In Situ Measurements of Arctic Low-Level Clouds: Microphysical Properties and Their Relationships With Aerosols, Journal of Geophysical Research: Atmospheres, 124, 1798–1822, https://doi.org/10.1029/2018JD029802, 2019.

Korhonen, H., Carslaw, K. S., Spracklen, D. V., Riley, D. A., and Ström, J.: A global model study of processes controlling aerosol size distribu-
625   tions in the Arctic spring and summer, Journal of Geophysical Research Atmospheres, 113, 1–20, https://doi.org/10.1029/2007JD009114, 2008.

Kuang, C., McMurry, P. H., and McCormick, A. V.: Determination of cloud condensation nuclei production from measured new particle formation events, Geophys. Res. Lett., 36, https://doi.org/10.1029/2009GL037584, 2009.

Lauber, A., Kiselev, A., Pander, T., Handmann, P., and Leisner, T.: Secondary ice formation during freezing of levitated droplets, J. Atmos.
630   Sci., 75, 2815–2826, https://doi.org/10.1175/JAS-D-18-0052.1, 2018.

Law, K. S. and Stohl, A.: Arctic Air Pollution: Origins and Impacts, Science, 315, 1537–1540, https://doi.org/10.1126/science.1137695, 2007.

Leaitch, W. R., Korolev, A., Aliabadi, A. A., Burkart, J., Willis, M. D., Abbatt, J. P., Bozem, H., Hoor, P., Köllner, F., Schneider, J., Herber, A., Konrad, C., and Brauner, R.: Effects of 20-100nm particles on liquid clouds in the clean summertime Arctic, Atmos. Chem. Phys., 16,
635   11 107–11 124, https://doi.org/10.5194/acp-16-11107-2016, 2016.

Liu, Y., Key, J. R., Ackerman, S. A., Mace, G. G., and Zhang, Q.: Arctic cloud macrophysical characteristics from CloudSat and CALIPSO, Remote Sens. Environ., 124, 159–173, https://doi.org/10.1016/j.rse.2012.05.006, 2012.

Lowe, S. J., Partridge, D. G., Davies, J. F., Wilson, K. R., Topping, D., and Riipinen, I.: Key drivers of cloud response to surface-active organics, Nature Comm., 10, 5214, https://doi.org/10.1038/s41467-019-12982-0, 2019.

640   Maturilli, M. and Kayser, M.: Arctic warming, moisture increase and circulation changes observed in the Ny-Ålesund homogenized radiosonde record, Theor. Appl. Climatol., 130, 1–17, https://doi.org/10.1007/s00704-016-1864-0, 2017.

Mauritsen, T., Sedlar, J., Tjernström, M., Leck, C., Martin, M., Shupe, M., Sjogren, S., Sierau, B., Persson, P. O., Brooks, I. M., and Swietlicki, E.: An Arctic CCN-limited cloud-aerosol regime, Atmos. Chem. Phys., 11, 165–173, https://doi.org/10.5194/acp-11-165-2011, 2011.

McFarquhar, G. M., Ghan, S., Verlinde, J., Korolev, A., Strapp, J. W., Schmid, B., Tomlinson, J. M., Wolde, M., Brooks, S. D., Cziczo,
645   D., Dubey, M. K., Fan, J., Flynn, C., Gultepe, I., Hubbe, J., Gilles, M. K., Laskin, A., Lawson, P., Leaitch, W. R., Liu, P., Liu, X., Lubin, D., Mazzoleni, C., Macdonald, A.-M., Moffet, R. C., Morrison, H., Ovchinnikov, M., Shupe, M. D., Turner, D. D., Xie, S., Zelenyuk, A., Bae, K., Freer, M., and Glen, A.: Indirect and Semi-direct Aerosol Campaign, Bull. Amer. Meteor. Soc., 92, 183–201, https://doi.org/10.1175/2010BAMS2935.1, 2011.

McFiggans, G., Artaxo, P., Baltensperger, U., Coe, H., Facchini, M. C., Feingold, G., Fuzzi, S., Gysel, M., Laaksonen, A., Lohmann, U.,
650   Mentel, T. F., Murphy, D. M., O'Dowd, C. D., Snider, J. R., and Weingartner, E.: The effect of physical and chemical aerosol properties
      on warm cloud droplet activation, Atmos. Chem. Phys., 6, 2593–2649, https://doi.org/10.5194/acp-6-2593-2006, 2006.

Mertes, S., Verheggen, B., Walter, S., Connolly, P., Ebert, M., Schneider, J., Bower, K. N., Cozic, J., Weinbruch, S., Baltensperger, U.,
      and Weingartner, E.: Counterflow Virtual Impactor Based Collection of Small Ice Particles in Mixed-Phase Clouds for the Physico-
      Chemical Characterization of Tropospheric Ice Nuclei: Sampler Description and First Case Study, Aerosol Sci. Technol., 41, 848–864,
655   https://doi.org/10.1080/02786820701501881, 2007.

METEK GmbH: uSonic-3 Omni Ultrasonic anemometer user manual, 2013.

Mitchell, J. M.: Visual range in the polar regions with particular reference to the Alaskan Arctic, J. Atmos. Terr. Phys., pp. 195–211, 1956.

Moore, R. H., Bahreini, R., Brock, C. A., Froyd, K. D., Cozic, J., Holloway, J. S., Middlebrook, A. M., Murphy, D. M., and
      Nenes, A.: Hygroscopicity and composition of Alaskan Arctic CCN during April 2008, Atmos. Chem. Phys., 11, 11 807–11 825,
660   https://doi.org/10.5194/acp-11-11807-2011, 2011.

Nguyen, Q. T., Glasius, M., Sørensen, L. L., Jensen, B., Skov, H., Birmili, W., Wiedensohler, A., Kristensson, A., Nøjgaard, J. K., and
      Massling, A.: Seasonal variation of atmospheric particle number concentrations, new particle formation and atmospheric oxidation capac-
      ity at the high Arctic site Villum Research Station, Station Nord, Atmos. Chem. Phys., 16, 11 319–11 336, https://doi.org/10.5194/acp-16-
      11319-2016, 2016.

665   Nomokonova, T., Ebell, K., Löhnert, U., Maturilli, M., and Ritter, C.: The influence of anomalous atmospheric conditions at Ny-Ålesund on
      clouds and their radiative effect, Atmos. Chem. Phys. Discuss., 20, 1–34, https://doi.org/10.5194/acp-2019-985, 2019a.

Nomokonova, T., Ebell, K., Löhnert, U., Maturilli, M., Ritter, C., and O'Connor, E.: Statistics on clouds and their relation to thermodynamic
      conditions at Ny-Ålesund using ground-based sensor synergy, Atmos. Chem. Phys., 19, 4105–4126, https://doi.org/10.5194/acp-19-4105-
      2019, 2019b.

670   Noone, K. J., Ogren, J. A., Heintzenberg, J., Charlson, R. J., and Covert, D. S.: Design and calibration of a counterflow virtual impactor for
      sampling of atmospheric fog and cloud droplets, Aerosol Sci. Technol., 8, 235–244, https://doi.org/10.1080/02786828808959186, 1988.

Ogren, J. A., Heintzenberg, J., and Charlson, R. J.: In-situ sampling of clouds with a droplet to aerosol converter, Geophys. Res. Lett., 12,
      121–124, https://doi.org/10.1029/GL012i003p00121, 1985.

Ovadnevaite, J., Ceburnis, D., Martucci, G., Bialek, J., Monahan, C., Rinaldi, M., Facchini, M. C., Berresheim, H., Worsnop, D. R., and
675   O'Dowd, C.: Primary marine organic aerosol: A dichotomy of low hygroscopicity and high CCN activity, Geophys. Res. Lett., 38,
      L21 806, https://doi.org/10.1029/2011GL048869, 2011.

Patoulias, D., Fountoukis, C., Riipinen, I., and Pandis, S. N.: The role of organic condensation on ultrafine particle growth during nucleation
      events, Atmos. Chem. Phys., 15, 6337–6350, https://doi.org/10.5194/acp-15-6337-2015, 2015.

Pedregosa, F., Varoquaux, G., Gramfort, A., Michel, V., Thirion, B., Grisel, O., Blondel, M., Prettenhofer, P., Weiss, R., Dubourg, V.,
680   Vanderplas, J., Passos, A., Cournapeau, D., Brucher, M., Perrot, M., and Duchesnay, E.: Scikit-learn: Machine Learning in Python, Journal
      of Machine Learning Research, 12, 2825–2830, 2011.

Pekour, M. S. and Cziczo, D. J.: Wake capture, particle breakup, and other artifacts associated with counterflow virtual impaction, Aerosol
      Sci. Technol., 45, 748–754, https://doi.org/10.1080/02786826.2011.558942, 2011.

Santachiara, G., Piazza, M., and Belosi, F.: Aerosol Scavenging during the Early Growth Stage of Ice Crystal Formation, Atmospheric and
685   Climate Sciences, 08, 395–409, https://doi.org/10.4236/acs.2018.84026, 2018.

Schmale, J., Kos, G., Jefferson, A., Yum, S. S., Sellegri, K., Gysel, M., Fröhlich, R., Poulain, L., Nenes, A., Keskinen, H., Artaxo, P., Pöhlker, C., Kalivitis, N., Bougiatioti, A., Frank, G., Matsuki, A., O'Dowd, C., Pöschl, U., Park, M., Picard, D., Mihalopoulos, N., Prévôt, A. S. H., Decesari, S., Herrmann, H., Kulmala, M., Wiedensohler, A., Schlag, P., Henzing, B., Pöhlker, M. L., Herrmann, E., Baltensperger, U., Holzinger, R., Äijälä, M., Petäjä, T., Aalto, P., Bukowiecki, N., Henning, S., Ogren, J., Swietlicki, E., Carbone, S., Ovadnevaite, J., Frumau, A., Ehn, M., Kristensson, A., Stavroulas, I., Iwamoto, Y., Andreae, M. O., and Stratmann, F.: Long-term cloud condensation nuclei number concentration, particle number size distribution and chemical composition measurements at regionally representative observatories, Atmos. Chem. Phys., 18, 2853–2881, https://doi.org/10.5194/acp-18-2853-2018, 2018.

Schwarzenboeck, A., Heintzenberg, J., and Mertes, S.: Incorporation of aerosol particles between 25 and 850 nm into cloud elements: measurements with a new complementary sampling system, Atmos. Res., 52, 241–260, https://doi.org/10.1016/S0169-8095(99)00034-4, 2000.

Seinfeld, J. H. and Pandis, S. N.: Atmospheric Chemistry and Physics : From Air Pollution to Climate Change, John Wiley & Sons, Incorporated, New York, 3 edn., 2016.

Serreze, M. C. and Barry, R. G.: Processes and impacts of Arctic amplification: A research synthesis, Global and Planetary Change, 77, 85–96, https://doi.org/10.1016/j.gloplacha.2011.03.004, 2011.

Serreze, M. C. and Francis, J. A.: The Arctic Amplification Debate, Climatic Change, 76, 241–264, https://doi.org/10.1007/s10584-005-9017-y, 2006.

Sharma, S., Chan, E., Ishizawa, M., Toom-Sauntry, D., Gong, S. L., Li, S. M., Tarasick, D. W., Leaitch, W. R., Norman, A., Quinn, P. K., Bates, T. S., Levasseur, M., Barrie, L. A., and Maenhaut, W.: Influence of transport and ocean ice extent on biogenic aerosol sulfur in the Arctic atmosphere, Journal of Geophysical Research: Atmospheres, 117, D12 209, https://doi.org/10.1029/2011JD017074, 2012.

Shingler, T., Dey, S., Sorooshian, A., Brechtel, F. J., Wang, Z., Metcalf, A., Coggon, M., Mülmenstädt, J., Russell, L. M., Jonsson, H. H., and Seinfeld, J. H.: Characterisation and airborne deployment of a new counterflow virtual impactor inlet, Atmos. Meas. Tech., 5, 1259–1269, https://doi.org/10.5194/amt-5-1259-2012, 2012.

Shupe, M. D., Walden, V. P., Eloranta, E., Uttal, T., Campbell, J. R., Starkweather, S. M., and Shiobara, M.: Clouds at Arctic Atmospheric Observatories. Part I: Occurrence and Macrophysical Properties, Journal of Applied Meteorology and Climatology, 50, 626–644, https://doi.org/10.1175/2010JAMC2467.1, 2011.

Sotiropoulou, G., Sullivan, S., Savre, J., Lloyd, G., Lachlan-Cope, T., Ekman, A. M., and Nenes, A.: The impact of secondary ice production on Arctic stratocumulus, Atmos. Chem. Phys., 20, 1301–1316, https://doi.org/10.5194/acp-20-1301-2020, 2020.

Spiegel, J. K., Zieger, P., Bukowiecki, N., Hammer, E., Weingartner, E., and Eugster, W.: Evaluating the capabilities and uncertainties of droplet measurements for the fog droplet spectrometer (FM-100), Atmos. Meas. Tech., 5, 2237–2260, https://doi.org/10.5194/amt-5-2237-2012, 2012.

Ström, J., Umegård, J., Tørseth, K., Tunved, P., Hansson, H. C., Holmén, K., Wismann, V., Herber, A., and König-Langlo, G.: One year of particle size distribution and aerosol chemical composition measurements at the Zeppelin Station, Svalbard, March 2000-March 2001, Phys. Chem. Earth, 28, 1181–1190, https://doi.org/10.1016/j.pce.2003.08.058, 2003.

Struthers, H., Ekman, A. M., Glantz, P., Iversen, T., Kirkevåg, A., Mårtensson, E. M., Seland, and Nilsson, E. D.: The effect of sea ice loss on sea salt aerosol concentrations and the radiative balance in the Arctic, Atmos. Chem. Phys., 11, 3459–3477, https://doi.org/10.5194/acp-11-3459-2011, 2011.

Sumlin, B. J., Heinson, W. R., and Chakrabarty, R. K.: Retrieving the aerosol complex refractive index using PyMieScatt: A Mie computational package with visualization capabilities, J. Quant. Spec. Rad. Trans., 205, 127–134, https://doi.org/10.1016/j.jqsrt.2017.10.012, 2018.

Tobo, Y., Adachi, K., DeMott, P. J., Hill, T. C. J., Hamilton, D. S., Mahowald, N. M., Nagatsuka, N., Ohata, S., Uetake, J., Kondo, Y., and Koike, M.: Glacially sourced dust as a potentially significant source of ice nucleating particles, Nature Geoscience, 12, 253–258, https://doi.org/10.1038/s41561-019-0314-x, 2019.

Tunved, P., Ström, J., and Krejci, R.: Arctic aerosol life cycle: Linking aerosol size distributions observed between 2000 and 2010 with air mass transport and precipitation at Zeppelin station, Ny-Ålesund, Svalbard, Atmos. Chem. Phys., 13, 3643–3660, https://doi.org/10.5194/acp-13-3643-2013, 2013.

von der Weiden, S.-L., Drewnick, F., and Borrmann, S.: Particle Loss Calculator – a new software tool for the assessment of the performance of aerosol inlet systems, Atmos. Meas. Tech., 2, 479–494, https://doi.org/10.5194/amt-2-479-2009, 2009.

Weingartner, E., Nyeki, S., and Baltensperger, U.: Seasonal and diurnal variation of aerosol size distributions (10< D <750 nm) at a high-alpine site (Jungfraujoch 3580 m asl), Journal of Geophysical Research: Atmospheres, 104, 26 809–26 820, https://doi.org/10.1029/1999JD900170, 1999.

Wendisch, M., Macke, A., Ehrlich, A., Lüpkes, C., Mech, M., Chechin, D., Dethloff, K., Velasco, C. B., Bozem, H., Brückner, M., Clemen, H.-C., Crewell, S., Donth, T., Dupuy, R., Ebell, K., Egerer, U., Engelmann, R., Engler, C., Eppers, O., Gehrmann, M., Gong, X., Gottschalk, M., Gourbeyre, C., Griesche, H., Hartmann, J., Hartmann, M., Heinold, B., Herber, A., Herrmann, H., Heygster, G., Hoor, P., Jafariserajehlou, S., Jäkel, E., Järvinen, E., Jourdan, O., Kästner, U., Kecorius, S., Knudsen, E. M., Köllner, F., Kretzschmar, J., Lelli, L., Leroy, D., Maturilli, M., Mei, L., Mertes, S., Mioche, G., Neuber, R., Nicolaus, M., Nomokonova, T., Notholt, J., Palm, M., van Pinxteren, M., Quaas, J., Richter, P., Ruiz-Donoso, E., Schäfer, M., Schmieder, K., Schnaiter, M., Schneider, J., Schwarzenböck, A., Seifert, P., Shupe, M. D., Siebert, H., Spreen, G., Stapf, J., Stratmann, F., Vogl, T., Welti, A., Wex, H., Wiedensohler, A., Zanatta, M., and Zeppenfeld, S.: The Arctic Cloud Puzzle: Using ACLOUD/PASCAL Multiplatform Observations to Unravel the Role of Clouds and Aerosol Particles in Arctic Amplification, Bull. Amer. Meteor. Soc., 100, 841–871, https://doi.org/10.1175/BAMS-D-18-0072.1, 2019.

Wex, H., Huang, L., Zhang, W., Hung, H., Traversi, R., Becagli, S., Sheesley, R. J., Moffett, C. E., Barrett, T. E., Bossi, R., Skov, H., Hünerbein, A., Lubitz, J., Löffler, M., Linke, O., Hartmann, M., Herenz, P., and Stratmann, F.: Annual variability of ice-nucleating particle concentrations at different Arctic locations, Atmos. Chem. Phys., 19, 5293–5311, https://doi.org/10.5194/acp-19-5293-2019, 2019.

Willis, M. D., Leaitch, W. R., and Abbatt, J. P.: Processes Controlling the Composition and Abundance of Arctic Aerosol, Rev. Geophys., 56, 621–671, https://doi.org/10.1029/2018RG000602, 2018.

Yu, H., Ortega, J., Smith, J. N., Guenther, A. B., Kanawade, V. P., You, Y., Liu, Y., Hosman, K., Karl, T., Seco, R., Geron, C., Pallardy, S. G., Gu, L., Mikkilä, J., and Lee, S.-H.: New Particle Formation and Growth in an Isoprene-Dominated Ozark Forest: From Sub-5 nm to CCN-Active Sizes, Aerosol Sci. Technol., 48, 1285–1298, https://doi.org/10.1080/02786826.2014.984801, 2014.

Zábori, J., Rastak, N., Yoon, Y. J., Riipinen, I., and Ström, J.: Size-resolved cloud condensation nuclei concentration measurements in the Arctic: Two case studies from the summer of 2008, Atmos. Chem. Phys., 15, 13 803–13 817, https://doi.org/10.5194/acp-15-13803-2015, 2015.

Zheng, Y., Rosenfeld, D., and Li, Z.: Quantifying cloud base updraft speeds of marine stratocumulus from cloud top radiative cooling, Geophys. Res. Lett., 43, 11,407–11,413, https://doi.org/10.1002/2016GL071185, 2016.